UK Vertical Lift Network

4th Annual Technical Workshop

Shrigley Hall Hotel, Cheshire

7th – 9th April 2019

Supported by:

EPSRC

Pioneering research and skills

Programme & Book of Abstracts

Introduction

UK Vertical Lift Network: 4th Technical Workshop

Welcome to the UK VLN Technical Workshop, an annual event showcasing the UK's cutting edge research in rotary wing research. Now in its third year, this event provides a platform for technical discussions on all things *rotorcraft,* from whirl flutter to active twist. For the third year running, we meet at picturesque Shrigley Hall Country House, nestled in the Cheshire hills overlooking Greater Manchester to the north.

We would like to thank all our presenters, who have provided the abstracts contain herewith in. This year sees the large number of the VLN community in attendance – 38 in total. This is an increase on last year, which shows that we are moving on a positive gradient, growing the rotorcraft research community – one of the core aims of the Vertical Lift Network.

We have a very full programme of 17 presentations this year, spread over five technical sessions over the next two days:

- Session 1A: Aerodynamics
- Session 1B: Tilt Rotors
- Session 2: Design and Simulation
- Session 3A: Advanced Propellers
- Session 3B: Propulsion Systems

We once again welcome our colleagues from industry to the technical workshop. Leonardo Helicopters and DSTL are actively engaged in rotorcraft research and have on-going collaborations with academic partners within the VLN. This healthy interaction demonstrates that our field is truly impactful and naturally collaborative. We also welcome for the first time at the VLN technical workshop some new and old friends from ARA, BAe Systems, Sophrodyne, and Vertical Aerospace. We thank our industrial VLN members for their time, contributions, and interest.

The purpose of this workshop is not limited to the presentation of on-going research. It is also a forum to exchange views and promote new ideas in a relaxing environment. We anticipate that this will stimulate discussion and further catalyse the growth of rotorcraft research in the UK.

We do hope you enjoy the technical workshop.

Antonio Filippone & Nicholas Bojdo
The University of Manchester
April 2019

4th VLN Technical Workshop - Programme
Shrigley Hall, Cheshire, 7th-9th April 2019

Sunday 7th April

1400 onwards	Check-in to Shrigley Hall Hotel
1500 – 1730	Country Walk (please bring appropriate footwear)
1900	Evening meal

Monday 8th April

0900 – 0910	Introduction (AF)
0915 – 1245	**Technical Presentation Session 1**
1245 – 1330	Lunch
1330 – 1500	**Technical Presentation Session 2**
1330 – 1800	VLN Meeting No. 25 (students may relax)
1900	Evening meal

Tuesday 9th April

0900 – 1300	**Technical Presentation Session 3**
1230 – 1330	Lunch
1330 – 1800	MENTOR meeting (students may depart after lunch)
1800	Close

The 4th Annual UK Vertical Lift Network Technical Workshop

Shrigley Hall Hotel, Cheshire

7-9th April 2019

BAT - University of Bath
BRI - University of Bristol
GLA - University of Glasgow
LEO - Leonardo Helicopters
LIV - University of Liverpool
MAN - University of Manchester
SOP - Sophrodyne

UK Vertical Lift Network

Final Programme

Monday 8th April

0900 - 0915	**Keynote**	Antonio Filippone	MAN	*Introduction : Update on the UK Vertical Lift Network*
0915 - 0945	**Aerodynamics**	Federico Rovere	GLA	*Brown-out and white-out modelling*
0945 - 1015		Samuel Bull	BAT	*Compound Transient Aerofoil Motions*
1015 - 1045		Richard Brown	SOP	*Understanding the Vortex Ring State through Experiment, Numerics and Theory*
1045 - 1115	Coffee Break			
1115 - 1145	**Tilt Rotors**	Wesley Appleton	MAN	*Aeromechanics modelling of tilt rotor aircraft*
1145 - 1215		Dami Adeyemi	BAT	*Whirl flutter modelling for active control*
1215 - 1245		Chris Mair	BRI	*Stability analysis of whirl flutter in non-linear gimballed rotor-nacelle*
1245 - 1330	Lunch Break			
1330 - 1400	**Design and Simulation**	Thomas Fitzgibbon	GLA	*Assessing rotor designs based on Navier-Stokes CFD predictions*
1400 - 1430		Tao Zhang	GLA	*Toward optimisation of compound rotorcraft*
1430 - 1500		Ben Woods	BRI	*SABRE: Shape adaptive blades for rotorcraft efficiency*
1500 - 1530		Wajih Memon	LIV	*Vestibular Motion Fidelity Requirements for Helicopter-Ship Operations*
1530 - 1800	**VLN Meeting #25**	All VLN Members		*See separate Agenda distributed by Florent DeHaeze*
1900 - 2100	Evening Meal			

Tuesday 9th April

0900 - 0930	**Advanced Propellers**	Ross Higgins	GLA	*Investigation of Propeller Flutter*
0930 - 1000		Angel Zarev	GLA	*Experimental Investigation of two-bladed propeller in yaw*
1000 - 1030		Dale Smith	MAN	*Aerodynamics of a counter rotating propeller with locked blade row*
1030 - 1100	Coffee Break			
1100 - 1130	**Propulsion Systems**	Matthew Ellis	MAN	*Reduced-Order Modelling of Mineral Dust Deposition in Turboshaft Engine Hot Sections*
1130 - 1200		Lewis Wiley	LEO	*Rotorcraft Hybrid Power Feasibility Study*
1200 - 1230		Yongjie Shi	GLA	*Helicopter rotor thickness noise control using unsteady force excitation*
1230 - 1300		Edward Yap	BRI	*Towards model development for helicopter inceptor dynamics*
1300 - 1330	Lunch Break			
1330 - 1800	**MENTOR Meeting**	All Mentor partners		*See separate programme distributed by George Barakos*

List of Attendees

Organisation	Name
Manchester	**Antonio Filippone**
	Nicholas Bojdo
	Wesley Appleton
	Matt Ellis
	Dale Smith
	Dionysios Klaudatos
Glasgow	**George Barakos**
	Thomas Fitzgibbon
	Ross Higgins
	Federico Rovere
	Yongjie Shi
	Angel Zarev
	Tao Zhang
Bristol	**Djamel Rezgui**
	Brano Titurus
	Ben Woods
	Edward Yap
	Chris Mair
Liverpool	**Mark White (VLN only)**
	Wajih Memon
Bath	**Jon du Bois**
	Samuel Bull
	Dami Adeyemi
BAe Systems	Khosru Rahman
Leonardo	**Florent DeHaeze**
	Lewis Wiley
	Alan Daniel
DSTL	**Richard Markiewicz**
	Neil Taylor
Sophrodyne	Richard Brown
ARA	**Andrew McCallum**
ATI	**Stuart Gates**
Taylor Aerospace	**Paul Taylor (VLN only)**
Vertical Aerospace	Michael Darcy
	Simon Harper
Hybrid Air Vehicles	**Carl Sequeira (VLN only)**

Technical Workshop Group shot (top) and VLN walk around Shrigley Hall (bottom), May 2017

Whirl Flutter Modelling for Active Control

Dami A. Adeyemi, David J. Cleaver, Jonathan L. du Bois
University of Bath, Department of Mechanical Engineering

Within the landscape of tiltrotor technology, dynamic instabilities such as whirl flutter are increasingly problematic for future generations of V/STOL aircraft. Aeroelastic coupling of pitching/yawing modes in typical propeller-nacelle-wing configurations remain a significant limiter of the range, speed, fuel efficiency and payload capabilities of these aircraft. Early proprotor flutter research centred on passive solutions that mitigated flutter by making adjustments to tiltrotor designs and their vibration damping/absorption subsystems - the design shift to bulkier wings for increased torsional stiffness being a good example. More recently, consideration has been given to active solutions using control feedback loops to achieve flexible flutter mitigation by manipulating tiltrotor system conditions in real-time. Empirical works on swashplate control schemes [1] [2] highlight the feasibility of such solutions, and recent experimental treatment of wing flaps by Gandhi et al [3], have been able to demonstrate practical applications that justify further exploration.

In modelling whirl flutter, multibody analysis tools like CAMRAD II, RCAS and Dymore facilitate high-level analysis of rotorcraft systems through the use of detailed nonlinear finite element theory (FEM), minimal top-level modelling approximations, and exact kinematics of rigid body and frame motions among others [4] [5] [6]. While these models provide great insight and fidelity, the associated high computational requirements are not optimal for active control development, where high speed computations are needed for practical development purposes [7]. In the work presented here, reduced order models (ROM) are developed and experimentally validated for two configurations, a simple gimbal configuration and a wing-mounted proprotor, with the intention of providing a suitable simulation environment for the investigation of active control technologies. The ultimate aim is to experimentally demonstrate the efficacy of the control techniques derived using these models.

The first configuration considered is a reduced scale 4-blade windmilling propeller mounted onto a gimbal allowing for rotation in the pitch/yaw directions (Fig. 1). Critical flutter velocities are observed in a wind tunnel for airspeeds up to $15 ms^{-1}$, for a range of 8 spring-extension combinations producing torsional stiffness between 0.01-0.08Nm at the gimbal. The model is based on the work presented by R. L.

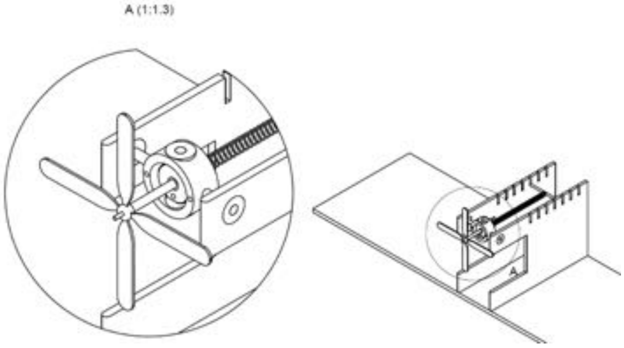

Figure 1: Test Rig for Propeller-Nacelle System

Bielawa for a propeller-nacelle (PN) system [8]. Initially a quasi-steady, linearised model was used, with aerodynamics derived under the assumption of small angles and state-space modelling used in eigenvalue analysis to determine stability boundaries. Flutter boundaries for this model however, were shown to underestimate the critical flutter speed observed in practice by roughly $10 ms^{-1}$ over the entire test range, and the viscous damping was replaced by a nonlinear damping model to better represent the experiment. A value for the Coulomb friction acting in the bearings was identified by calibrating the model at a single pitch stiffness, K_θ = 0.027. This produced a flutter boundary in good agreement with the experimental data across the entire pitch stiffness range. The

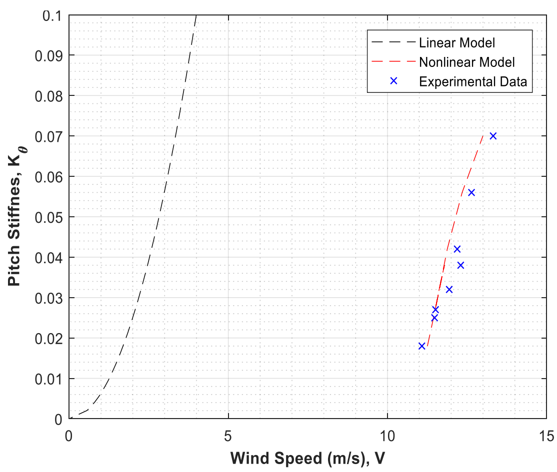

Figure 2: PN Model Validation

experimental results are compared with the two models in Fig. 2, where the nonlinear model is seen to lie within 1% of the experimental data for all test cases.

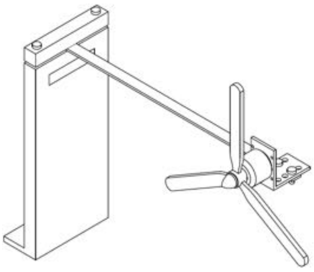

(a) FE Validation

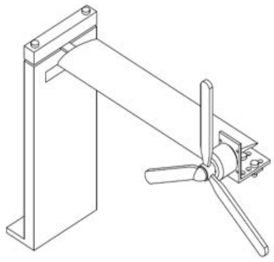

(b) Wing Aerodynamics Validation

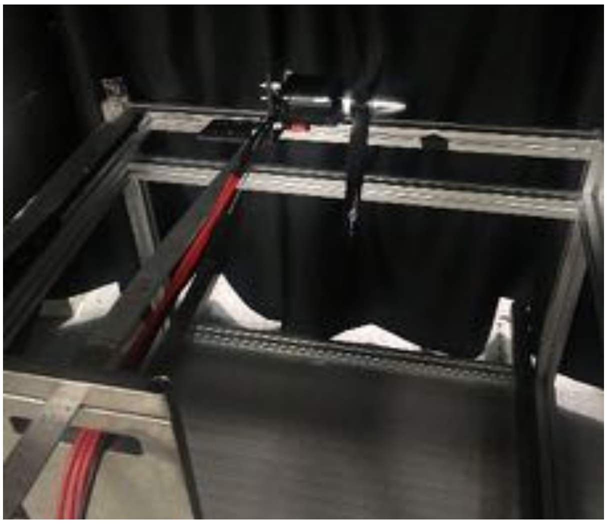

(c) Test Rig

Figure 3: Test Rigs for Propeller-Nacelle-Wing Systems

The second configuration is a more representative propeller-nacelle-wing (PNW) system, seen in Fig.3. To convert from the PN model to a PNW equivalent, extra degrees of freedom (DOFs) relating to wing plunge, surge and spanwise bending were added to the proprotor model, with wing surge velocity dynamics at the propeller ignored. The characteristic equations were derived using coordinate frame kinematics commonly used in robotics applications [9], and verified in so far as they simplify to Bielawa's PN equations upon removal of the new DOFs. The wing itself is included in the state-space model using finite element methods for a cantilevered *Euler-Bernoulli* beam. Finally, aerofoil strip theory is used to simulate the aerodynamic forcing. Two sets of experimental validations are performed. The first, shown in Fig. 3(a, c), is intended to validate the new FE modelling while minimising aerodynamic wing effects. The second, shown in Fig. 3(b) incorporates an aerofoil to validate the strip theory modelling.

While the windmilling propeller of the first configuration used an empirically-derived relationship between advance ratio and wind speed, the second configuration uses a powered proprotor, and linearised blade element momentum theory (BEMT) is used to predict the thrust variation with RPM (Fig. 4a). Preliminary testing indicates that the model's force derivations are in the correct range (~20N peak thrust at 4800RPM, 0ms^{-1} wind, seen in Fig. 4b).

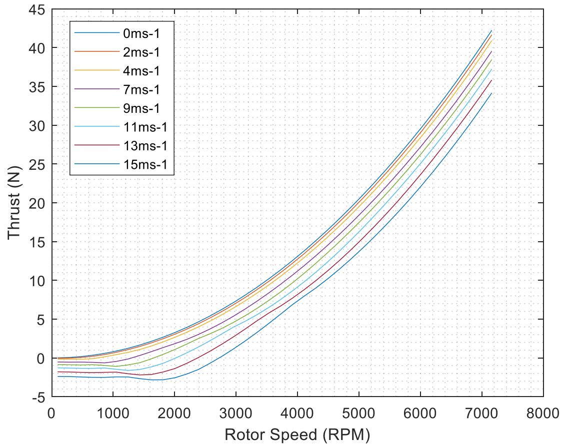

(a) Simulated Thrust Vs Rotor Speed, for 0-15ms^{-1} wind speed

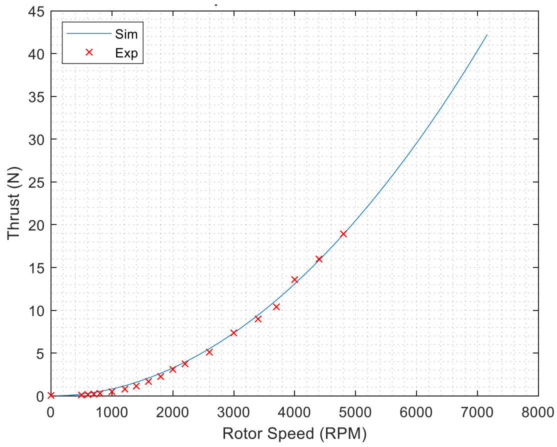

(b) Preliminary Test Results at 0ms^{-1} wind speed

Figure 4: Analytical Data for the PNW System

Results to date indicate that a good agreement can be found between the low order models and experimental behaviour, and that the models are well suited to control development for active control of whirl flutter. Future work will apply these models to develop a multistate feedback controller using an active flap on the wing to mitigate whirl flutter. Using active control surfaces on the wing instead of smart rotor technologies makes for a much simpler implementation with less risk of critical failures. A flap/wing chord ratio of

0.25, and a span ratio of 0.5 are anticipated, and the results of the simulation will be used in the implementation of an experimental proof-of-concept for the techniques. This will be an important step in realising efficient whirl flutter mitigation strategies for future rotorcraft.

References

[1] K.-I. Nasu, "Tilt-rotor flutter control in cruise flight," NASA Ames Research Center, Moffett Field, CA, United States, 1986.

[2] J. V. &. I. Chopra, "Stabilizing Pylon Whirl Flutter on a Tilt-Rotor Aircraft," in *32nd Structures, Structural Dynamics, and Materials Conference*, Baltimore,MD,U.S.A., 1991.

[3] R. S. E. H. &. F. G. Jinho Paik, "Active Tiltrotor Whirl–Flutter Stability Augmentation Using WIng-Flaperon and Swash-Plate Actuation," *Journal of Aircraft,* vol. 44, no. 5, pp. 1439-1446, 2007.

[4] W. Johnson, "Technology Drivers in the Development of CAMRAD II," Johnson Aeronautics, Palo Alto, California, 1994.

[5] O. A. Bauchau, "Dymore User's Manual," School of Aerospace Engineering, Georgia Institute of Technology, Atlanta, GA, USA, 2006.

[6] J. J. &. J. Cotrell, "A Demonstration of the Ability of RCAS to Model Wind Turbines," National renewable Energy Laboratory, Golden, Colorado, 2003.

[7] R. M. M. &. J. Alotaibi, "Efficient Implementation of a Helicopter Hingless Rotor Model with Active Trailing Edge Flaps for Control Design," *UKACC 12th International Conference on Control,* p. 93, Sept 2018.

[8] R. L. Bielawa, Rotary Wing Structural Dynamics and Aeroelasticity, American Institute of Aeronautics and Astronautics, 2006.

[9] R. P. P. &. C. N. Stevenson, "Kinematics of Robot Wrists," *The International Journal of Robotics Research,* vol. 2, no. 1, pp. 31-38, 1983.

Aeromechanics Modelling of Tiltrotor Aircraft

Wesley Appleton[1], Antonio Filippone and Nicholas Bojdo
School of Mechanical, Aerospace and Civil Engineering
The University of Manchester, UK

1 Introduction

The tiltrotor configuration meets the demand of future high-speed rotorcraft by tilting the rotor drive-shafts in-flight. They deliver the speed, range and performance of turboprop fixed-wing aircraft together with the low-speed operability of traditional helicopters. This research has focused on understanding the fundamental behaviour of tiltrotor aircraft and the underpinning aeromechanics. The flight regime studied has been the conversion corridor - the flight envelope that bounds the airspeed as a function of the shaft angle. More specifically, understanding when and why the inherent rotary-wing and fixed-wing behaviours are exemplified depending on the particular combination of shaft angle and airspeed. This was achieved by first establishing a generic aeromechanics model of a tiltrotor aircraft. Due to the largely unpopulated literature regarding tiltrotor aircraft, the model configuration was based on the well-documented Bell XV-15 tiltrotor. The aircraft was trimmed in steady and level flight by solving the longitudinal and vertical equations of motion and observing the trim characteristics.

2 Tiltrotor Aeromechanics Model

The generic aircraft model was discretised into the major aerodynamic components - fuselage, rotors, wing and empennage. In the research, only the longitudinal flight characteristics of the tiltrotor were studied and therefore the vertical stabilisers were omitted from the empennage configuration leaving only the horizontal stabiliser. The total aerodynamic loads on the airframe were then the sum of the individual component loads. These loads were subsequently substituted into the equations of motion to determine the resultant accelerations of the airframe. The geometric and aerodynamic configuration data for the Bell XV-15 tiltrotor aircraft was taken from References [1–3].

The aerodynamic loads from the rotors on the airframe were calculated using a fourth-order Runge-Kutta time-integrated state-space system until a steady, periodic solution was obtained. The induced flow was modelled using the prescribed three-state dynamic inflow model of Pitt and Peters [4]. The equations of motion of the gimballed rotorhead were derived by summing the inertial, spring and aerodynamic moments on the rotorhead from all blades. The resulting coupled, second-order linear differential equations were solved as a system of first-order differential equations describing the gimbal states - the tilt angles and their respective rates.

The fixed-wing loads were calculated using strip theory. The wing configuration data and lift, drag and moment coefficients were taken from Reference [2] to calculate the two-dimensional section loads. The spacial position of the half-wing relative to the cg was found from three successive rotations through the sweep, twist and dihedral angles. The aerodynamic loads were then integrated along the half-wing span from an effective root to effective tip. The longitudinal and vertical loads from the wing were then doubled to account

[1]Corresponding author email: wesley.appleton@manchester.ac.uk

for the entire wing and the lateral loads cancelled to zero. The horizontal tail loads were also calculated using the preceding method. At this time, the downwash from rotor induced flow was neglected.

3 Preliminary Conversion Corridor Results

During conversion flight, the rotor experiences a diverse aerodynamic environment. Therefore, the rotor model had to be validated to ensure sufficiently accurate performance estimates were obtained through the full shaft angle range. The performance comparison through the conversion corridor against experimental data is presented in Figure 1. The results show a good level of agreement overall, particularly as the shaft is tilted towards aeroplane mode as shown in Figure 1a. In helicopter mode, Figure 1b, the required power is under-predicted, especially towards high-thrust settings. The under-prediction of the required power was accounted for from blade model aerodynamic differences, absence of a transonic drag-rise model and also from the low-order, prescribed induced flow model. The results were, however, deemed sufficiently accurate for preliminary performance estimations.

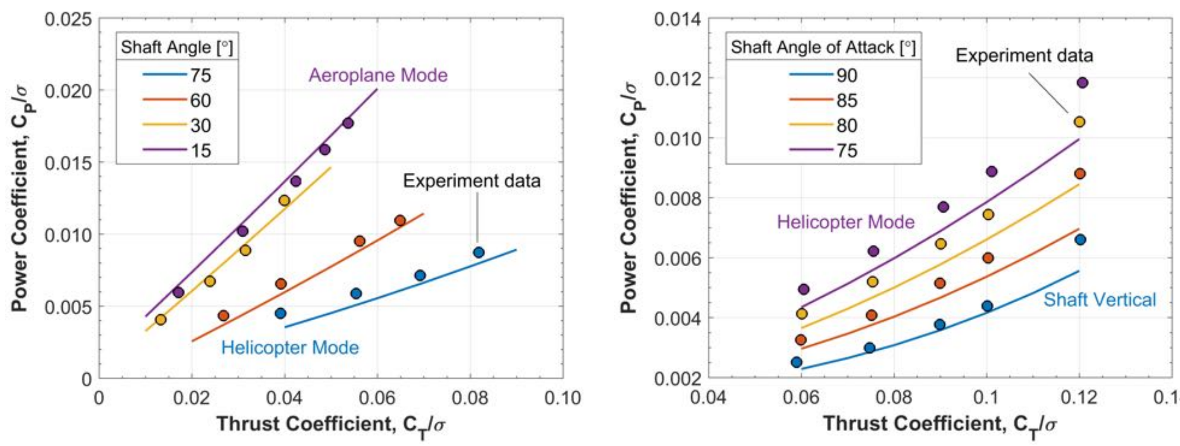

(a) Rotor model performance validation through conversion flight against data from Johnson [6] at a tip-speed ratio of 0.32.

(b) Rotor model performance correlation in helicopter mode against data from Betzina [5] at a tip-speed ratio of 0.17.

Figure 1: Correlation of the rotor model performance results against experimental data.

The aircraft was trimmed in steady and level flight at a fixed shaft angle over a range of airspeeds. The trim quantities to be determined were the aircraft angle of attack, collective pitch setting and longitudinal control stick displacement. The trim solution was obtained using a multivariate Newton-Raphson method with a central-difference scheme implemented to approximate the partial derivatives in the Jacobian matrix. To improve the convergence and stability of the scheme, particularly towards the corridor boundaries, under-relaxation was used. The trim sweep was calculated for shaft angle intervals of 15° and airspeed intervals of 10kn. The imposed constraints on the trim state are summarised in Table 1.

Table 1: Constraints imposed on the trim state.

Trim Quantity	Constraint Limits
Pitch attitude	$\pm 20°$
Required power fraction	1
Gimbal tilt angles	$\pm 12°$
Longitudinal control stick	± 1

The predicted conversion corridor boundaries are presented in Figure 2a and compared against those in Reference [1]. The upper limit is well predicted but overlooks the structural limit of the aircraft as this was not accounted for in the aircraft model. The largest discrepancy is observed at the lower boundary with the airspeed limit under-predicted towards helicopter mode and over-predicted towards aeroplane mode. The lower limit in aeroplane mode was determined by the required angle of attack and also the control stick displacement, the latter was found to be the constraining parameter. Above an angle of attack of approximately 10°, the elevator became ineffective. Therefore, no pitch-up moment could be generated and the aircraft was consequently untrimmable, owing to the over-predicted lower boundary.

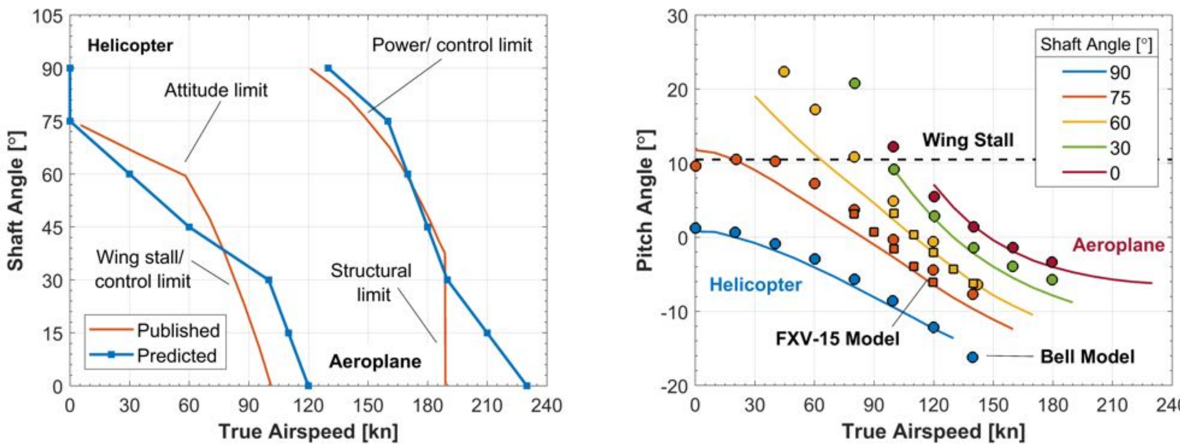

(a) Predicted conversion corridor boundaries against the published conversion corridor [1].

(b) Predicted pitch attitude in trimmed flight through the conversion corridor against the Bell flight dynamics model [2] and FLIGHTLAB XV-15 (FXV-15) model [7].

Figure 2: Predicted conversion corridor boundaries and trimmed pitch attitude in conversion flight.

The trimmed pitch attitude during conversion flight is presented in Figure 2b, showing a good level of agreement overall. The trimmed pitch attitude is well predicted for shaft angles of 90° , 30° and 0°, however, there is an evident under-prediction at low-and-moderate airspeeds at shaft angles of 75° and 60°. This was attributed to the absence of a downwash model of the induced flow. This would cause a reduced angle of attack at the affected wing sections and result in a download on the airframe. Both these effects would require an increase in the pitch angle to counteract them. Furthermore, the inflexion of the pitch attitude curves show a transition from rotary-wing to fixed-wing behaviour. Furthermore, in the region where the pitch attitude varies approximately linearly with airspeed, the behaviour is neither that of a traditional helicopter or aeroplane. This observed behaviour is unique to tiltrotor aircraft. This will be investigated to determine the underlying principles that answer the observed trends, providing a deeper understanding of this future, high-speed rotorcraft.

References

[1] M. Maisel, "Tilt Rotor Research Aircraft Familiarization Document," *NASA Technical Memorandum X-62, 407*, 1975.

[2] P. Harendra, M. Joglekar, T. Gaffey, and R. Marr, "V/STOL Tilt Rotor Study - Volume V: A Mathematical Model For Real Time Flight Simulation of the Bell Model 301 Tilt Rotor Research Aircraft," *Bell Helicopter Company Report No. 301-099-001*, 1973.

[3] S. Ferguson, "A Mathematical Model for Real Time Flight Simulation of a Generic Tilt-Rotor Aircraft," *NASA Contractor Report CR-166563*, 1988.

[4] D. Pitt and D. Peters, "Rotor Dynamic Inflow Derivatives and Time Constants from Various Inflow Models," *9th European Rotorcraft Forum*, pp. 1–24, 1983.

[5] M. Betzina, "Rotor Performance of an Isolated Full-Scale XV-15 Tiltrotor in Helicopter Mode," *American Helicopter Society Aerodynamics, Acoustics, and Test and Evaluation Technical Specialists Meeting*, pp. 1–12, 2002.

[6] W. Johnson, "An Assessment of the Capability to Calculate Tilting Prop-Rotor Aircraft Performance, Loads and Stability," *NASA Technical Paper 2291*, 1984.

[7] G. Padfield, *Helicopter Flight Dynamics: Including a Treatment of Tiltrotor Aircraft*. Wiley, third ed., 2018.

Compound Transient Aerofoil Motions and the Principle of Linear Superposition

S.C. Bull, I. Gursul and D.J. Cleaver.
Dept. of Mechanical Engineering, University of Bath, BA2 7AY, UK.

Rotorcraft blades operate in a naturally unsteady environment due to a combination of flapping, pitching and rowing motions coupled with unsteady disturbances. In scenarios where the flow remains attached over the aerofoil, linear theory can provide reasonable predictions of the unsteady loads. However this theory breaks down when the aerofoil operates close to or beyond its static stall angle and where the unsteadiness becomes sufficiently large. In these scenarios flow separation will occur above the aerofoil which subsequently rolls up into coherent vortical structures and, due to their highly non-linear behaviour, have been the subject of research for decades. In the rotorcraft community this is known as dynamic stall and is characterised by significant hysteresis and large lift and nose-down pitching moment increases, far beyond the static value [1]. Research efforts in many fields have sought to characterise the behaviour of these structures to better inform reduced-order models [2] to provide tools for designers to either avoid, supress or enhance dynamic stall events.

Recent focus in the aerodynamic community has shifted from periodic to transient aerofoil motions in pitch, plunge and surge to better understand vortex-aerofoil and vortex-vortex interactions [3]. Previous measurements taken at The University of Bath [4] have shown that the change in lift during a transient plunging motion, indicated by the grey region in Figure 1, is almost identical for pre-stall (α_0=5°, shown in blue) and post-stall (α_0=20°, shown in red) angles of attack despite the significant differences in initial flow field. Once the motion has ended however the pre-stall aerofoil rapidly decays to a flat lift response, whereas the post-stall aerofoil displays additional lift peaks caused by large-scale vortex shedding - alternating vortices formed at the leading and trailing edge of the aerofoil. This finding along with similar transient studies [5] then poses the question; if the lift response during motion is largely insensitive to the initial flow state, could a succession of transient motions be predicted by the linear superposition of a single event, even where large-scale vortex shedding is present?

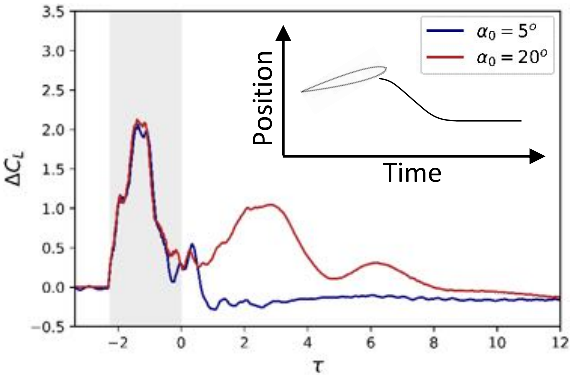

Figure 1: Transient plunging aerofoil lift response

A. TRANSIENT MOTION

This question has been tested for various successive transient plunging aerofoil motions, termed compound motion. A typical result is shown in Figure 2. The duration of the second motion is indicated by the grey region and the linear superposition prediction taken from Figure 1 is shown with dashed lines. Excellent agreement can be seen between the experimental result and the linear superposition prediction for both cases, even despite the highly non-linear vortical flow observed in the post-stall case. The maximum lift during the second motion increases by 50% for the post-stall aerofoil, highlighting the significance of investigating these events and the importance of being able to model them. The presentation will consider more cases including the effect of time delay between motions, angle of attack and amplitude. The accuracy of the linear superposition will be quantified and supported by flow field measurements to explain the underlying flow behaviour.

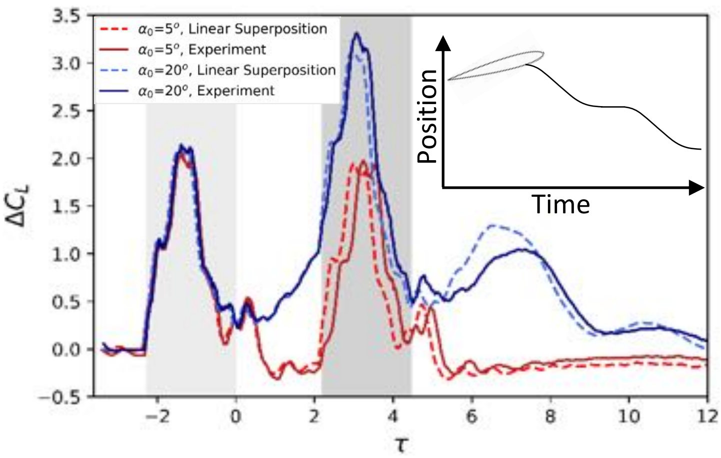

Figure 2: Compound transient lift response

The concept of linear superposition can also be applied to many transient plunging motions. Figure 3 shows that linear superposition can predict with reasonable accuracy the significant lift increase that can occur for post-stall wings during these scenarios.

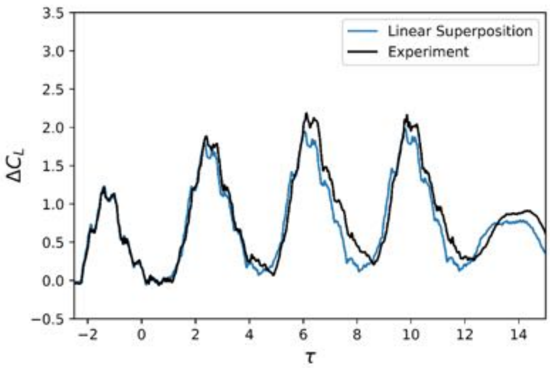

Figure 3: Compound motion of four transient events, α_0=20°

B. PERIODIC MOTION

The logical extension from multiple motions is periodic motions. The motions considered were sinusoidal and the basic starting point is a single sinusoid defined in the inset of Figure 4. This produces the lift response shown in Figure 4 for a post-stall (α_0=15°) aerofoil. Linear superposition of this single sinusoid produces a reasonable prediction of the periodic response, see Figure 5. Figure 6 presents the comparison of measured and estimated mean lift and lift amplitude across a wide range of Amplitudes and Strouhal numbers. This shows that the prediction holds reasonably well for all amplitudes up to a Strouhal number of around 0.20, with lower amplitudes being preferable, indicating it is more precise where added-mass effects are less dominant. In the presentation the full load time histories and select PIV measurements will be shown. These results provide a fundamental understanding into compound motion effects and have potential impact for the modelling community.

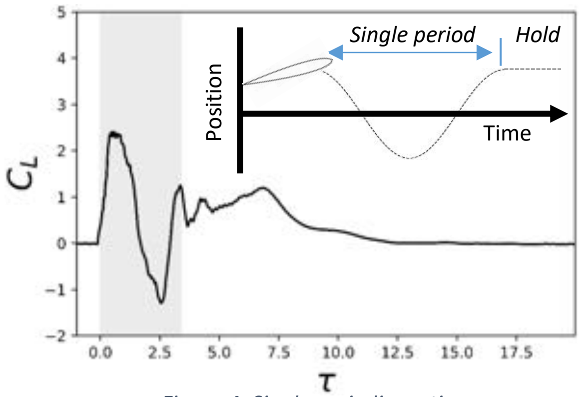

Figure 4: Single periodic motion

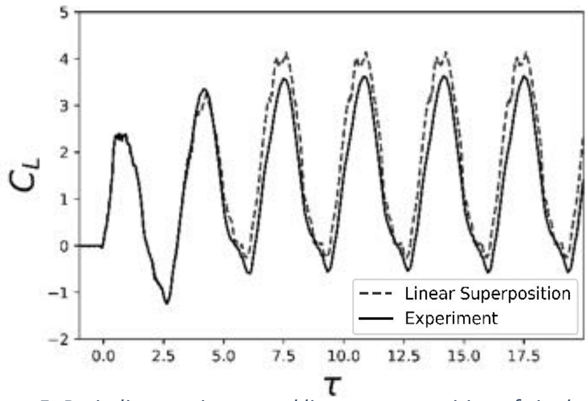

Figure 5: Periodic experiment and linear superposition of single motion

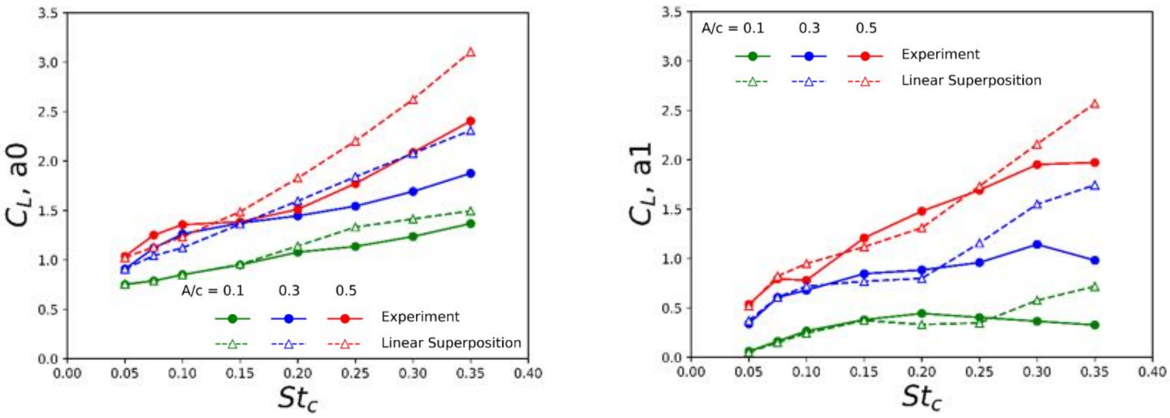

Figure 3: Comparison between linear superposition of single period and periodic experiment for a) mean lift and b) lift amplitude

[1] W. J. McCroskey, “The Phenomenon of Dynamic Stall,” *NASA Tech. Memo. 81264*, 1981.

[2] J. G. Leishman, “Challenges in Modeling the Unsteady Aerodynamics of Wind Turbines,” in *21st ASME Wind Energy Symposium and the 40th AIAA Aerospace Sciences Meeting*, 2002, pp. 1–28.

[3] M. V. Ol and H. Babinsky, “Unsteady Flat Plates: a Cursory Review (Invited - AVT202 special session),” *54th AIAA Aerosp. Sci. Meet.*, no. January, 2016.

[4] S. C. Bull, N. Chiereghin, I. Gursul, and D. J. Cleaver, “Unsteady Aerodynamics of a Transient Plunging Airfoil.”

[5] K. Mulleners, P. Mancini, and A. R. Jones, “Flow Develpment on a Flat-Plate Wing Subjected to a Stremwise Acceleration,” *AIAA J.*, vol. 55, no. 6, 2017.

Reduced-Order Modelling of Mineral Dust Deposition in Turboshaft Engine Hot Sections

Matthew Ellis, Nicholas Bojdo, and Antonio Filippone
University of Manchester, Oxford Road, Manchester, M13 9PL, United Kingdom

I. Introduction

As rotorcraft perform near ground manoeuvres in dry, arid environments, significant amounts of dust on the ground can become lofted by the downwash from the main rotor, rapidly enveloping the entire airframe in a process known as *'brownout'*. These dust clouds often have concentrations which are several orders of magnitude greater than those experienced even during severe sandstorms. For example, sandstorm dust concentrations can peak at up to 10 mg/m^3, whilst the brownout cloud concentration produced by the V-22 Osprey during a landing manoeuvre can be as high as 3500 mg/m^3. The result of this is that large quantities of particulate from this cloud are ingested by the engines, something which has been cited as a contributing factor to multiple rotorcraft accidents, some of these fatal. Protection against particle ingestion can be afforded through the employment of an Engine-Air Particle Separator (EAPS) system which can remove the majority of larger particles through inertial separation or direct filtration. Despite this a quantity of the ingested particulate still enters the engine where it can cause significant damage, with extensive erosion and abrasion of the compressor stages occurring before particulate is heated and softened in the latter compressor stages and the combustion chamber. The softened particulate that exits the combustor then encounters the high pressure turbine nozzle guide vanes (NGV) where it can deposit on the vane pressure surfaces. The extent of this deposition is a complex function of the physical properties of the particulate such as its size and shape, its behaviour under heating, the geometry of the vane and the flow velocities and temperatures around it. The end result of this deposition is an increase in the physical thickness of the vane and a reduction in the nozzle throat area. This constriction in the flow-path area through the NGV stage manifests as a decrease in the overall core mass flow rate, causing a reduction in the surge margin of the engine. This reduction continues as the deposit builds up, to the point at which the mass flow rate though the compressor is no longer sufficient to sustain the adverse pressure gradient, resulting in engine surge and potentially failure. Due to the abnormally high dust concentrations involved with brownout, this degradation can occur in a matter of just minutes, making it a serious safety issue for rotorcraft operators, as evidenced by the fatal crash of a V-22 Osprey in Hawaii due to deposition induced engine surge and failure [1].

Historically, the models developed to predict NGV damage due to deposition have focused on providing a detailed three-dimensional representation of the deposit morphology and therefore the reduction in the nozzle throat area. These have generally taken the form of sub-system and component scale high-fidelity CFD simulations, in which the full extent of the complex deposit topology and therefore throat area restriction could be predicted. Whilst this detailed prediction of the throat area reduction is informative, there is doubt over whether so much detail is required from a model. Ultimately, it is the minimum throat area through the NGV passage that restricts the core flow and therefore predicting the deposit structures across the entire pressure surface of the vane in three dimensions is potentially a waste of computational resources. However, the main downside of these high fidelity models is the resulting computation times which at a minimum can be of the order hours, increasing potentially to days. For reactive operations such as those carried out by military and search and rescue organisations, flight in brownout conditions cannot always be mitigated against and waiting hours to determine whether a platform can operate a mission safely is not suitable. As a result, there is significant motivation from these operators for the development of low-order models which can be used to make rapid fly or no-fly decisions based upon a set of inputs relating to the mission profile, platform and environment.

II. Methodology

This work aims to develop a reduced order model that can be used to give rapid operational capability predictions of rotorcraft platforms operating in brownout conditions for a given duration in a known dust cloud concentration. The product of these two parameters gives the *'dose'* of particulate and is fast becoming the standard by which the amount of particulate ingested by gas turbine engines is quantified. From a known dose, the total dust mass that is ingested can be determined. The aim of this reduced order model is to predict the mass proportion of the ingested dust which eventually deposits and builds up on a vane for a given dose of particulate. The reduced order model is built around the use of two-dimensional CFD simulations, with the results of these used to develop statistical relationships describing the probabilistic behaviour of a particle sticking upon impact with a vane. This probability of sticking is defined as the capture probability, the likelihood that a particle sticks and remains stuck to the vane. As shown in Figure 1 this can be split into two distinct sub-probabilities, termed the Interaction and Retention probabilities. These probabilities are described as functions of the non-dimensional inertial and thermal stokes numbers, parameters which relate to the inertial and thermal response properties of the particle respectively and are in general proportional to its size. Where possible, *'generalised'* forms of these parameters are being sought such that the interaction and retention probabilities can be described using a single function for a range of flow and particle properties, with the only variable being the geometry with which the particle interacts. These relatively simple statistical functions can be applied to particle size distributions of real life dusts in order to assess the mass fraction of particulate ingested that ultimately deposits on a vane. Figure 1 shows how by expressing particle size distribution functions in terms of the non-dimensional parameters, we can determine the interaction and retention probabilities for each diameter in the size distribution. This gives us two new functions, the area under which represent the mass fraction of ingested dust that interacts and is retained by the vane. Finally, by multiplying these two probabilities, we can obtain the capture efficiency for the particle size distribution, with the area under this curve representing the total mass that is captured and therefore sticks to the NGV.

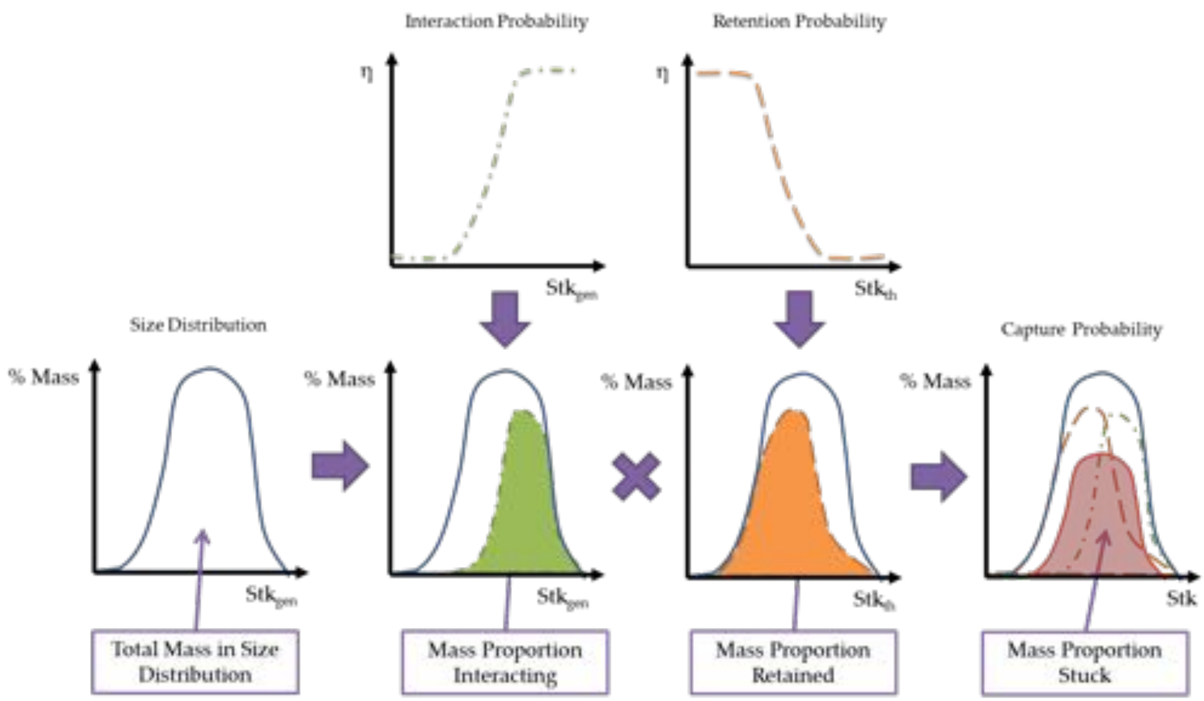

Fig. 1 The reduced order modelling strategy being employed in this work, showing how probability functions for the interaction and retention probabilities can be combined to give the capture efficiency of a dust distribution.

III. Results

A. Interaction Probability

As a particle transits an NGV stage, the trajectory it follows and therefore whether it interacts with a vane depends on the response of the particle to the inertial forces which act upon it. This is often described using the Stokes number, the ratio between the particle and fluid response times and is a function of the velocity and viscosity of the gas and the density and diameter of the particle. The dominant force which influences a particle to deviate from the flow streamlines and interact with the vane is the drag force, a function of the relative flow between the particle and fluid and therefore the particle relative Reynolds number. Over the course of its transit to the vane, a particle can experience a range of drag coefficients as its relative Reynolds number varies due to the presence of an additional inertial drag force at high flow Reynolds numbers. These drag coefficients can be significantly different to those predicted by the linear drag law upon which the Stokes number is derived . As a result, the interaction efficiency for a particular Stokes number will vary depending upon the Reynolds number of the fluid it resides in.

In this model we utilise a new form of the generalised Stokes number, first derived by Israel & Rosner [2] which can be applied to normalise the interaction efficiency of an NGV for a range of flow Reynolds numbers. This generalised form of the Stokes number gives a better prediction of the particle drag force by integrating the drag coefficient experienced over the particle trajectory. The result is a parameter which can be related to the interaction probability for all Reynolds numbers. The example shown in Figure 2b demonstrates how the interaction efficiency can be normalised with the generalised Stokes number for the three different continuous phase Reynolds numbers in Figure 2a. Curve fitting to this normalised data gives the interaction efficiency as a function of the generalised Stokes number. This function is dependent only upon the vane geometry and constitutes a vast reduction in the number of dependent parameters for the interaction efficiency.

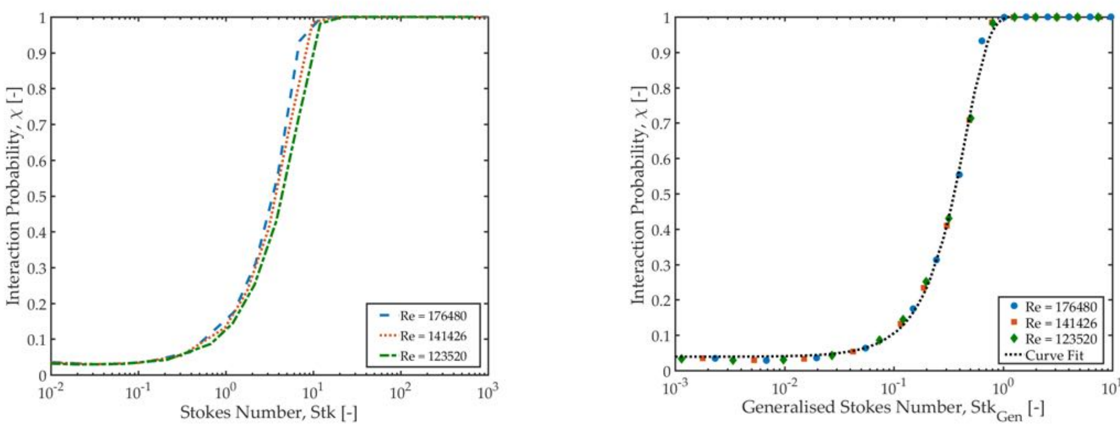

(a) Stokes Number **(b) Generalised Stokes Number**

Fig. 2 Effect of the Generalised Stokes number (b) in normalising freestream Reynolds number variation in the Interaction Efficiency seen when the standard Stokes number (a) is used

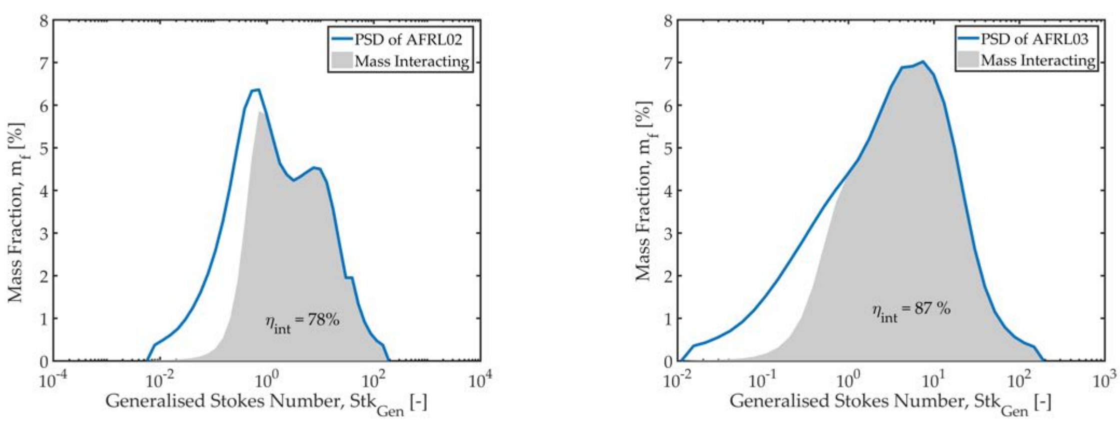

(a) AFRL02 **(b) AFRL03**

Fig. 3 Application of the Generalised Stokes number and Interaction probability to the size distribution of AFRL02 (a) and AFRL03 (b)

In line with the method shown in Figure 1, the relationship between the generalised Stokes number and interaction efficiency can be used to determine the mass proportion of a dust distribution that interacts with a vane. Firstly, using the curve fit function from Figure 2b the interaction probability is determined for the generalised Stokes number corresponding to each particle size in the distribution. This is then multiplied by the mass frequency in each size band to give the mass fraction of each generalised Stokes number that interacts with the NGV. Integrating under this curve then gives the proportion of the ingested particulate mass which interacts with the vane. As this is for the generalised Stokes number, this is valid for all flow conditions and is dependent only on the vane geometry. An example application of this process is shown in Figure 3 for the AFRL02 and 03 standardised test dusts [3] with the NGV geometry of the GE-E^3 engine [4].

B. Retention Probability

The retention probability of a particle defines its propensity to stick to a vane upon interaction. It is a complex function of the elastic, adhesive and thermal properties of the particle and substrate it interacts with. Of these factors, past work has identified the dominance that temperature has in the determination of a particles state of matter, with higher temperatures leading to a particle softening, having reduced elastic moduli and yield strength and therefore a greater probability of depositing. This can be related to the thermal response properties of the particle and whether it has sufficient time to equilibrate with its surrounding gas as it transits across the NGV. It is for this reason that the retention probability is proposed to be a function of a ’Thermal’ Stokes number. This is defined as the ratio of the particle thermal response time and the velocity response time of the gas, although further work is required to generalise this parameter for a range of flow conditions, making it suitable for use in the reduced order model.

In order to describe this sticking process of a particle on a vane, the numerical particle deposition model of Bons et.al [7] has been employed, incorporating the impact, adhesion, rebound and removal by shear flow phases of the particle wall interaction. Despite multiple models describing this behaviour existing, this particular formulation represents a significant step in improving the physical processes involved in particle deposition, by accounting for the plastic deformation of a particle upon impact. This has been noted to have significant effect on the prediction of the coefficient of restitution as when assuming perfectly elastic impacts, the amount of energy that the particle stores during the impact phase is over-predicted. In reality, a threshold exists at which a maximum elastic energy storage is reached and any additional energy is used to deform the particle plastically. Crucially, and unlike for elastic collisions, this additional plastic energy cannot be recovered during the rebound phase, reducing the amount of energy available for rebound and therefore the coefficient of restitution of the particle, making it more likely to deposit. In addition to this, the temperature dependence of deposition is incorporated by assuming that the yield strength of the particle reduces linearly with increasing temperature, therefore accounting for the gradual softening of the particle as it is heated which results in an increased likelihood of plastic deformation and therefore deposition.

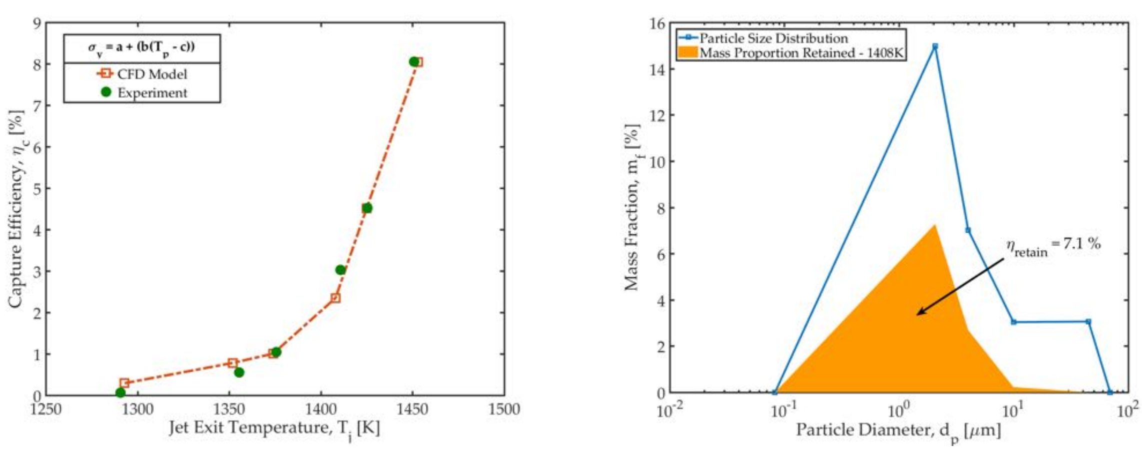

(a) (b)

Fig. 4 Validation of the particle deposition model with increasing gas temperature (a) and the result of its subsequent application to determine the Retention efficiency of the size distribution in the validation case from [7] (b)

This model has been developed into a user defined subroutine and applied as a boundary condition in the CFD models used to develop the statistical functions underpinning the reduced order method. Figure 4 shows the validation of this model against the experimental data set of Ai and Fletcher for the deposition of sub-bituminous ash particles entrained in a jet with variable temperature incident on an inclined metal coupon [8]. Work is ongoing to apply this model to the types of mineral dust ingested during brownout. Therefore, the results of this validation case have been used to show how the retention probability of a particle size distribution can be determined in a similar way the interaction probability. As work is also still ongoing to determine an appropriate non-dimensional parameter to describe the retention probability, we express this instead as a function of the particle diameter for the purposes of demonstrating the model. Multiplying the retention probability for each diameter by its corresponding mass fraction in the particle size distribution, the mass fraction of each size band that is retained can be determined as shown in Figure 4b for the 1408K validation case shown in Figure 4a. Again, by integrating under this curve, the proportion of the total mass of particulate ingested by the engine that is retained and therefore the overall retention probability of the NGV can be determined. Finally, combining this with the interaction efficiency gives the final output of the model, the overall capture probability of the vane which represents the proportion of the particulate mass ingested which sticks to the vane.

References

[1] Sweetman, O., "Hawaii V-22 Accident Investigation Points To New Ingestion Issue," , 2015.

[2] Israel, R., and Rosner, D. E., "Use of a Generalized Stokes Number to Determine the Aerodynamic Capture Efficiency of Non-Stokesian Particles from a Compressible Gas Flow," *Aerosol Science and Technology*, Vol. 2, No. 1, 1982, pp. 45–51. doi:10.1080/02786828308958612, URL `http://www.tandfonline.com/doi/abs/10.1080/02786828308958612`.

[3] Phelps, A. W., and Pfledderer, L., "Development of a naturalistic test media for dust ingestion CMAS testing of gas turbine engines," *Thermal Barrier Coatings IV*, 2014, p. 2. URL `http://dc.engconfintl.org/thermal_barrier_iv/29`.

[4] Timko, L. P., "Energy Efficient Engine high pressure turbine component test performance report," Tech. rep., National Aeronautics and Space Administration, Jan. 1984.

[5] Singh, S., and Tafti, D., "Particle deposition model for particulate flows at high temperatures in gas turbine components," *International Journal of Heat and Fluid Flow*, Vol. 52, 2015, pp. 72–83. doi:10.1016/j.ijheatfluidflow.2014.11.008.

[6] Brach, R., Dunn, P., and Li, X., "Experiments and Engineering Models of Microparticle Impact and Deposition," *Journal of Adhesion*, 2000. URL `http://www3.nd.edu/~pdunn/www.dunnpapers/00BDLjadh.pdf`.

[7] Bons, J. P., Prenter, R., and Whitaker, S., "A Simple Physics-Based Model for Particle Rebound and Deposition in Turbomachinery," *Journal of Turbomachinery*, Vol. 139, No. 8, 2017.

[8] Ai, W., and Fletcher, T., "Computational Analysis of Conjugate Heat Transfer and Particulate Deposition on a High Pressure Turbine Vane," 2009, p. 13.

Assessing different rotor designs based on Navier-Stokes CFD predictions

Thomas A. Fitzgibbon * and George N. Barakos †

The advancement of rotor design is highly dependant on the accuracy of performance prediction tools. Accurate predictions lead to reduced uncertainties and give higher confidence in radical rotor designs. With the growth in computational power and development of CFD methods, improved rotor designs are likely to come from numerical simulation. Advanced planform shapes such as the BERP design [1], Blue-Edge blade [2] or new BOEING rotor blade [3], must be evaluated with modern CFD tools as a first step. The assumptions made by comprehensive rotor codes such as CAMRAD or HOST may lead to an inaccurate representation of the flow around more complex shapes, meaning that high fidelity CFD methods are required for simulations. The aim of this presentation is to evaluate CFD predictive capabilities for more advanced planform shapes in hover and high-speed forward flight, and to explore the differences in performance between different rotor blade designs.

For this purpose, we use the experimental data of Yeager et al. [4]. To our knowledge, this is the only experiment concerning advanced planform shapes, in the public domain. Two rotor blades were tested here, a rectangular planform (LBL) and a advanced planform with a paddle-shaped blade tip (LBERP). Both blades were simulated in this paper using the HMB3 solver of Glasgow University in hover and high-speed forward flight condition. However, only integrated loads experimental data is available for these blades. For this reason, the PSP rotor blade [5] is also simulated due to available surface pressure data. This presentation will be composed of two key parts: CFD validation and rotor design analysis, with a primary focus on advanced rotor blade planforms.

The hover and forward flight performance predictions for the LBL, LBERP and PSP blades are shown in figure 1. Very good agreement is obtained of the CFD performance predictions with experimental data. A detailed design analysis is performed based on the CFD results, that provides the causes for the performance trends of both blade designs. This includes surface pressure distributions, surface streamlines, and rotor disk loads (in forward flight) with sample results shown in figures 2- 4.

Acknowledgments: This work is funded by DSTL (Defence Science and Technology Laboratory), Project No. 74260. This work used the Cirrus UK National Tier-2 HPC Service at EPCC (http://www.cirrus.ac.uk). This work used the ARCHER UK National Supercomputing Service (http://www.archer.ac.uk).

References

[1] Perry, F., "Aerodynamics of the World Speed Record," *43rd Annual Forum of the American Helicopter Society*, St. Louis, Missouri, 1987.

[2] Rauch, P., Gervais, M., Cranga, P., Baud, A., Hirsch, J., Walter, A., and Beaumier, P., "Blue Edge (TM): The Design, Development and Testing of a New Blade Concept," *American Helicopter Society 67th Annual Forum*, Virginia Beach, Virginia, 2011.

[3] Boeing, "New Chinook Composite Blades Proven," 2017, http://www.boeing.com/features/2017/01/chinook-blades-01-17.page, Online; accessed 22-March-2018.

[4] Yeager Jr, W., Noonan, K., Singleton, J., Wilbur, M., and Mirick, P., "Performance and Vibratory Loads Data From a Wind-Tunnel Test of a Model Helicopter Main-Rotor Blade With a Paddle-Type Tip," Tech. rep., National Aeronuatics and Space Administration, 1997, NASA-TM-4754.

[5] Overmeyer, A. D. and Martin, P. B., "Measured Boundary Layer Transition and Rotor Hover Performance at Model Scale," *55th Aerospace Sciences Meeting*, Grapevine, Texas, 2017.

*PhD Student - t.fitzgibbon.1@research.gla.ac.uk - CFD Laboratory, School of Engineering, University of Glasgow, G12 8QQ, UK

†Professor - George.Barakos@glasgow.ac.uk - CFD Laboratory, School of Engineering, University of Glasgow, G12 8QQ, UK

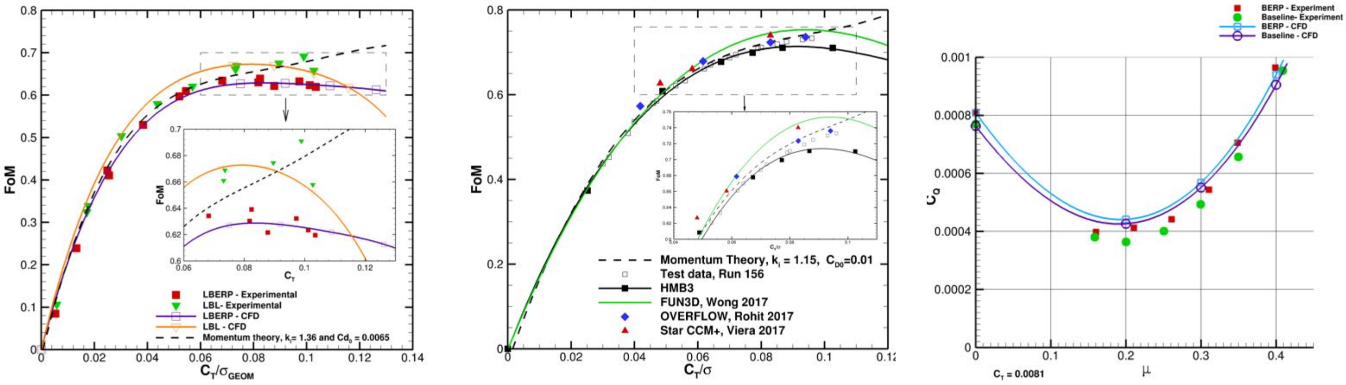

(a) Langley blades (hover), C_T/σ-FoM.

(b) PSP blade (hover), C_T/σ-FoM

(c) Langley blades (FF), $C_T = 0.0081$, μ-C_Q

Figure 1: Performance predictions for the Langley BERP, Langley Baseline and PSP blades, and comparisons with experimental data from Yeager et al. [4] and Overmeyer and Martin [5].

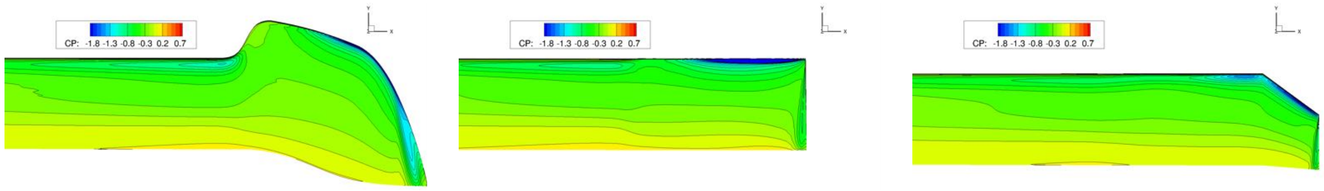

(a) LBERP

(b) LBL

(c) PSP

Figure 2: Surface pressure coefficient distributions across the blade tip for the LBERP, LBL and PSP blade designs at C_T=0.008.

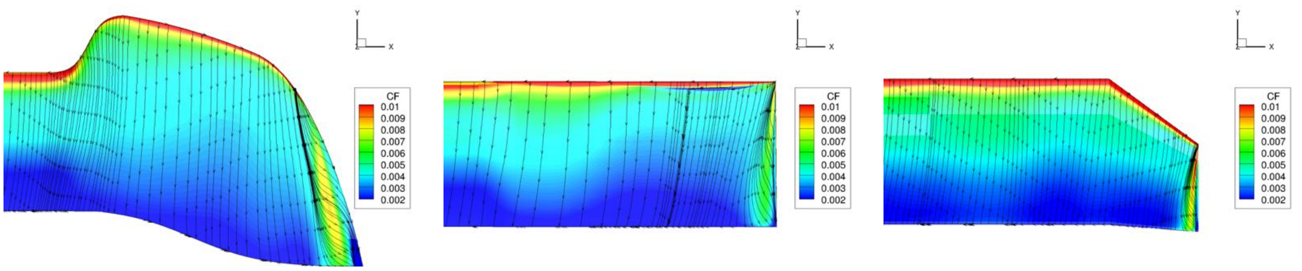

(a) LBERP

(b) LBL

(c) PSP

Figure 3: Surface skin friction coefficient distributions and surface skin friction lines across the blade tip for the LBERP, LBL and PSP blade designs at C_T=0.008.

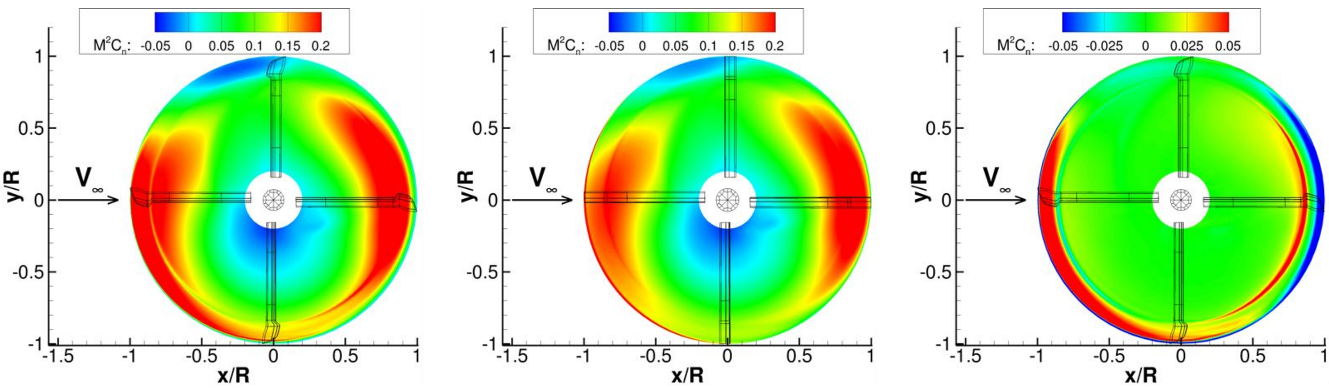

(a) LBERP, M^2C_N

(b) LBASELINE, M^2C_N

(c) LBERP-LBL, M^2C_N

Figure 4: Rotor disk normal force distributions for Langley BERP and Baseline blades at $C_T = 0.0081, \mu = 0.4$.

4th Vertical Lift Network Workshop, 8-9th April 2019, Cheshire, United Kingdom

Investigation of Propeller Stall Flutter

Ross J. Higgins * and George N. Barakos †

Propeller flutter manifests in a variety of different ways, including classic, stall and whirl flutter. Whirl and stall in particular, require detailed modelling of the aerodynamics and structural response of a propeller. In stall flutter, the non-linear aerodynamics is a result of the detached flow-field which triggers the aeroelastic excitation.

Successful capture of such aerodynamic interactions allows for increased accuracy in surface loads, and increased accuracy in predicting the resultant flutter boundary. From this base, and with the development of faster computing power, a time-marching aeroelastic method has been developed which couples Computational Fluid Dynamics (CFD) and Computational Structural Dynamics (CSD). Flutter of any type is a result of a fluid-structure interaction and the method was derived based on this assumption.

There has been many static experimental investigations conducted, all of which followed a similar test procedure in which the blade rotational velocity was increased at a fixed pitch angle [1, 2, 3, 4, 5]. In terms of numerical studies [6, 7, 8], all have focused on the inclusion of non-linear aerodynamics through unsteady dynamic stall models applied to two-dimensional sections. To date, no 3D aerodynamic and structural modelling using Computational Fluid Dynamics (CFD)/Computational Structural Dynamics (CSD) is reported for propeller stall flutter.

This investigation involved the full three-dimensional study of the Commander propeller[2]. This test case was selected due to the availability of experimental data and its application on an actual aircraft. The Commander propeller is three bladed and was designed by GE-DOWTY in the 1970's. The propeller is modelled in isolation, with periodicity in space assumed. The test conditions mirrored that of the experiment conducted by DOWTY in 1979 [2], in which the blade is accelerated from 1400 to 1750 RPM with a fixed pitch angle. The structural model for the Commander blades are based upon the assumption of a solid material blade. The linear mass distribution is calculated as a function of the cross-section area, with the blade inertia based upon the variation in cross-section area.

For this investigation, a comparison is made to the standard $URANS$ equations, coupled with the $k-\omega$ turbulence model, to the Scale-Adaptive Simulation (SAS) method. The SAS method produces an LES like solution, with modest computation resources, through the local adjustment of the von Karman length scale.

Presented in Figure 1 is the modal response for the third propeller mode for both the $URANS$ and SAS simulations. The SAS method suggests flutter, and a step change is seen during the acceleration. The ability of the SAS method to capture the vortex shedding (an example of the difference in flow-field visualisation is presented in Figure 2) allows for a greater variation in the surface loads which triggers the aeroelastic excitation.

The presentation will provide a full detail of the method and results of this investigation.

Acknowledgements

The support provided by DOWTY Propellers is gratefully acknowledged.

*PhD Student - r.higgins.1@research.gla.ac.uk - CFD Laboratory, School of Engineering, University of Glasgow, G12 8QQ, UK

†Professor - George.Barakos@glasgow.ac.uk - CFD Laboratory, School of Engineering, University of Glasgow, G12 8QQ, UK

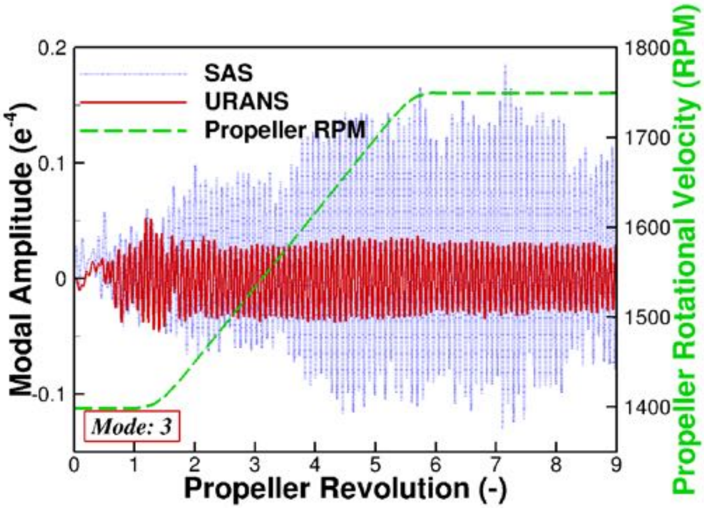

Figure 1: Modal amplitude response for third propeller mode for the *URANS* and *SAS* simulations.

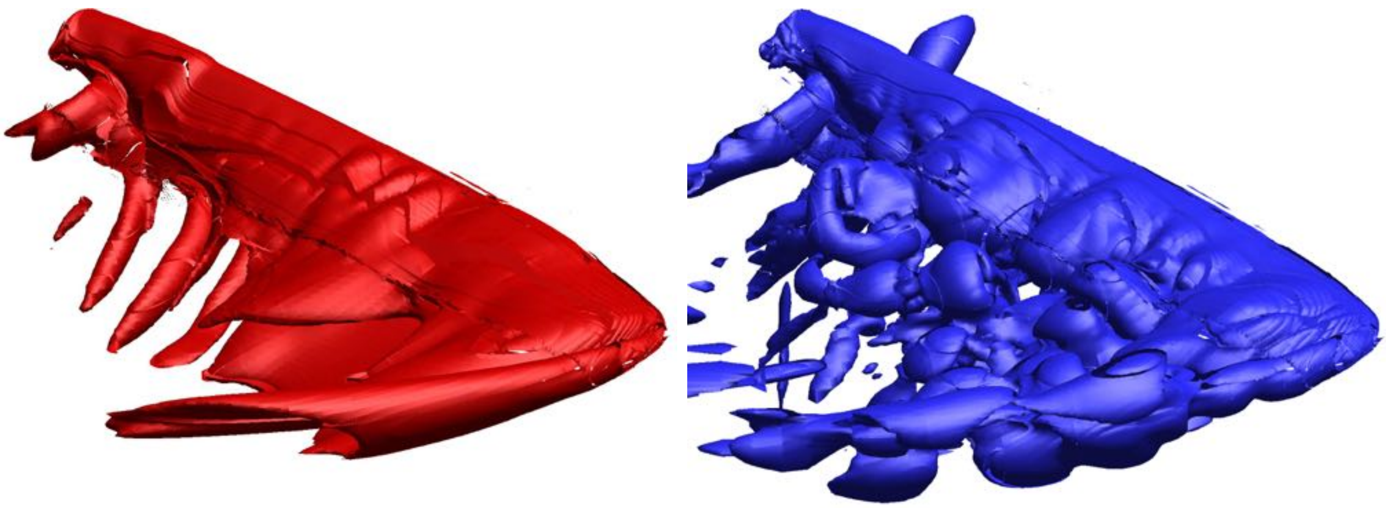

(a) *URANS*

(b) *SAS*

Figure 2: Flow visualisation using vorticity magnitude iso-surface of $|\omega| = 1.5$.

References

[1] Sterne, L., "Spinning Tests on Fluttering Propellers," *Aeronautical Research Council: Reports and Memoranda*, , No. 2022, 1945.

[2] Burton, P., "Straingauge Test Report on a Spin Test Carried out on a Type (c) R.305/3-82-F/6 Propeller on the Spinning Tower at the R.A.E. Farnborough, Hants." Tech. Rep. 093.1.592, DOWTY ROTOL LTD., 1979.

[3] Smith, A., "Analysis and Test Evaluation fo the Dynamic Stability of Three Advanced Turboprop Models at Zero Forward Speeds," Contractor Report 175025, National Aeronautics and Space Administration, 1985.

[4] Baker, J., "The effects of various parameters, including Mach number, on propeller-blade flutter with emphasis on stall flutter," Tech. Rep. 3357, National Advisory Commitee for Aeronautics, 1955.

[5] Hubbard, H., Burges, M., and Sylvester, M., "Flutter of thin propeller blades, including effects of Mach number, structural damping, and vibratory-stress measurements near the flutter boundaries," Tech. Rep. 3707, National Advisory Commitee for Aeronautics, 1956.

[6] Reddy, T. and Kaza, K., "Analysis of an Unswept Propfan Blade with a Semiempirical Dynamic Stall Model," Technical Memorandum, National Aeronautics and Space Administration, 1989.

[7] Delamore-Sutcliffe, D., *Modelling of Unsteady Stall Aerodynamics and Prediction of Stall Flutter Boundaries for Wings and Propellers*, Ph.D. thesis, University of Bristol, 2007.

[8] Ognev, V. and Rosen, A., "Influence of using various unsteady aerodynamic models on propeller flutter prediction," *Journal of Aircraft*, Vol. 48, No. 5, 2011.

Stability analysis of whirl flutter in a nonlinear gimballed rotor-nacelle system

Chris Mair[1], Dr Djamel Rezgui[2] and Dr Branislav Titurus[3]

Department of Aerospace Engineering,

University of Bristol, Queens Building, Bristol, UK

Summary

Whirl flutter is an aeroelastic instability that affects several vehicles, including tiltrotors. Both civilian and military tiltrotor operators are looking to maximise the capacity and speed of tiltrotor models, though it is not known how nonlinear effects scale with size. Furthermore, whirl flutter limits the maximum speed of current tiltrotor models [1] and therefore their productivity, heightening the importance of adequate modelling and prediction tools. This paper presents the stability analysis of a 9 degree-of-freedom gimballed rotor-nacelle system in both its original linear form and an adapted nonlinear variant featuring a structural nonlinearity. The nonlinearities investigated are polynomial stiffness profiles of both hardening and softening forms, resembling the relaxation and saturation in the stiffness of the rotor tilting joint/mechanism. The model is representative of a tiltrotor aircraft both in the features reflected in the modelling, and the parameter values used. Appropriate stability analysis methods are explained and used to demonstrate the "overhang" phenomenon, where nonlinearities cause whirl flutter behaviours to be possible in parameter regions where linear analysis has predicted stability.

The impact of nonlinearity on a tiltrotor wing-nacelle system's behaviour and stability are shown through the use of stability boundaries between structural design parameters. The importance of proper modelling and analysis methods is thus shown.

Introduction

Tiltrotors such as the ERICA tiltrotor shown in Figure 1 are a technology area of growing importance due to their potential solution of the airport congestion problem worldwide. If tiltrotors with the passenger capacity of a regional jet can be developed, then regional jet traffic can be offloaded from the runways and transferred to helipads that most airports are already equipped with. In addition to the fact that this desired size of tiltrotor is substantially larger than any existing models, a further challenge is ensuring accurate aeroelastic modelling to protect against an instability known as whirl flutter. The continual development of technology means that the new, larger tiltrotors will likely utilise newer, lighter materials and rotor systems with different per-rev frequencies. The prediction of coupling between destabilising modes therefore acquires significant uncertainty [1].

Whirl flutter in its most common context involves a rotor or propeller mounted in a wing nacelle, the hub of which whirls in a circle around its nominal un-deflected position. Aerodynamic forces acting on the blades and gyroscopic effects acting on the rotor as a whole can couple with wing modes to produce an unstable vibration which can damage or even destroy the aircraft structure. With their large and flexible blades, tiltrotors are particularly susceptible, and whirl flutter generally limits their maximum cruise speed.

[1] PhD Student, University of Bristol, chris.mair@bristol.ac.uk
[2] Lecturer in Aerospace Engineering, University of Bristol, djamel.rezgui@bristol.ac.uk
[3] Lecturer in Aerospace Engineering, University of Bristol, brano.titurus@bristol.ac.uk

Traditional eigenvalue analysis can be used to assess the stability of linear systems. However, for nonlinear systems bifurcation and continuation methods can give a more complete insight, particularly when stability boundaries are required.

Figure 1: ERICA tiltrotor concept

Models and stability methods

The authors previously investigated a nonlinear adaption of a simple linear whirl flutter model [2] originally derived by Reed [3], where the "overhang" phenomenon was first identified. The model used in this research is a 9-DoF model presented by Johnson [4]. The model uses a modal representation of various rotor and wing degrees of freedom, with quasi-static aerodynamics derived from strip theory. Both the cyclic and collective motions of the flapping and lead-lag degrees of freedom are modelled. Flap-wise, chord-wise and torsional bending of the wing are also considered. The model was encoded in MATLAB in ode45 format, and AUTO (DST) [5] by Coetzee was used to perform the continuation analysis. Time simulations were also used to corroborate calculated findings. Validation of the model was achieved through comparison of the implemented model's eigenvalues with a plot given by Johnson in [4], and is shown in Figure 2.

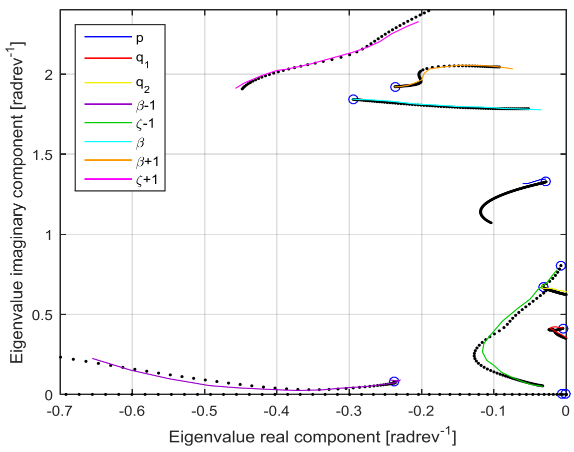

Figure 2: Eigenvalue Argand diagram plot for Johnson model implementation validation

Numerical continuation and bifurcation techniques calculate the steady-state solutions of a dynamical system as one of its parameters, called the continuation parameter, is varied [6]. The computed solutions construct a number of branches that can be either stable or unstable. To determine their stability, either an eigenvalue or Floquet analysis is carried out at each computed solution point, depending on the nature of the solution. For behaviours considered to be in equilibrium (fixed points), an eigenvalue analysis can be used (requiring local linearization in the case of a nonlinear system), whereas periodic behaviours (limit cycles) require Floquet theory to determine the stability [7].

For the nonlinear variation of Johnson's model, polynomial stiffness profiles were introduced to the wing torsion degree of freedom. Using an expression of the form $K(\psi)\psi = K_1\psi + K_2\psi^3 + K_3\psi^5$, hardening and softening behaviours could be affected and even combined, while still retaining control of the original linear stiffness. A one-parameter bifurcation diagram in airspeed (represented by the advance ratio μ) is shown in Figure 3.

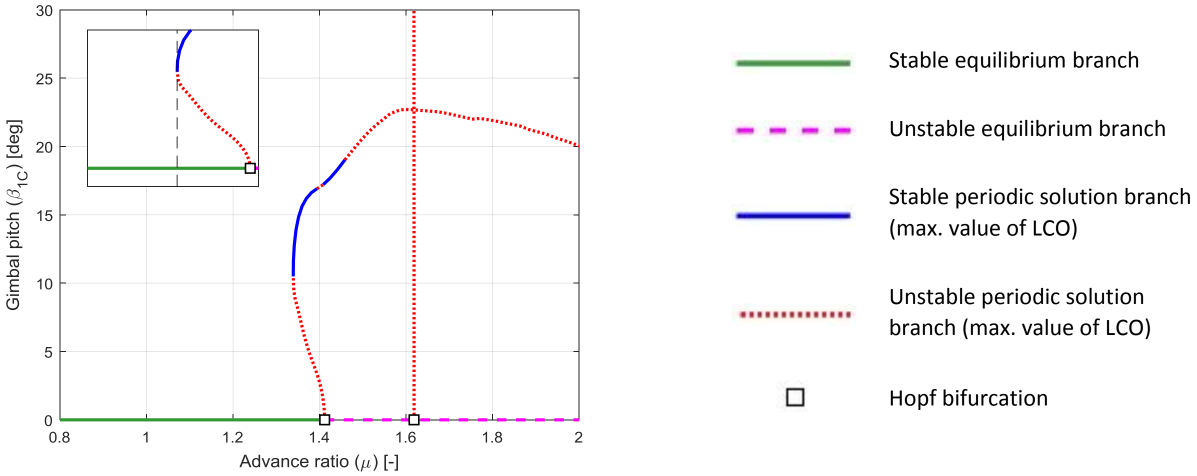

Figure 3: Bifurcation diagram showing continuation in advance ratio for a mixed cubic softening quintic hardening profile (K_1=3.595, K_2=-30, K_3=500). Inset shows extent of overhang over main branch

The Hopf bifurcation at μ=1.4 marks the onset of instability in the form of whirl flutter motions. Some stable (blue) portions of the periodic solution branches exist down to approximately μ=1.3, overhanging the stable main branch (green) which mirrors the predictions of linear stability analysis. Physically speaking, a sufficient perturbation of the rotor or nacelle will cause the system to encounter whirl flutter despite the prediction of stability. A further Hopf bifurcation is seen at approximately μ=1.6; the straightness of the branch is characteristic of linear systems and therefore probably does not involve the wing torsion degree of freedom.

Conclusions

A nonlinear adaption of a gimballed rotor-nacelle model by Johnson is analysed through continuation and bifurcation methods. Polynomial stiffness profiles of both hardening, softening and mixed forms are implemented in the wing torsion degree of freedom. Continuations in several parameters are performed and the results displayed in bifurcation diagrams. Different state projections are used to understand how the whirl flutter motions are manifested.

Overall, the impact and consequential importance of the modelling of system nonlinearities is demonstrated. An altered stability boundary - where the extent of overhang is fully taken in account - is to be presented at the event.

References:

[1] Acree C. W., Johnson W., Aeroelastic Stability of the LCTR2 Civil Tiltrotor, 2008
[2] Mair C., Rezgui D., Titurus B., “Nonlinear stability analysis of whirl flutter in a tiltrotor rotor-nacelle system”, Proc 34th European Rotorcraft Forum, Milan, 2017
[3] Reed W. H., Propeller-Rotor Whirl Flutter: A State-of-the-Art Review, 1965
[4] Johnson W., “Dynamics of tilting proprotor aircraft in cruise flight,” NASA Technical Note D-7677, 1974
[5] Coetzee, E., Krauskopf, B., Lowenberg, M.: The dynamical systems toolbox: Integrating AUTO into MATLAB, Proc. 16th US National Congress of Theoretical and Applied Mechanics USNCTAM2010-827, 2010
[6] Rezgui D., Lowenberg M. H., On the nonlinear dynamics of a rotor in autorotation: a combined experimental and numerical approach, 2015
[7] Kuchment P. A., Floquet Theory for Partial Differential Equations, 1993

QINETIQ UNIVERSITY OF LIVERPOOL [dstl]

Vestibular Motion Fidelity Requirements for Helicopter-Ship Operations in Maritime Rotorcraft Flight Simulations

Wajih A Memon*, Ieuan Owen and Mark D White
wajih.ahmed.memon@liverpool.ac.uk
Flight Science & Technology, The University of Liverpool, UK

The UK's Royal Navy and Royal Fleet Auxiliary regularly perform launch and recovery operations of helicopters to and from their ships. These operations are carried out in challenging conditions such as confined ship deck space, irregular ship motion, sea spray and unsteady airflows, posing a high risk to the helicopter, ship and the crew. Together these elements form the Helicopter Ship Dynamic Interface (HSDI) environment [1]. To determine the limitations of the safe operability of helicopters to ships, a safety envelope is constructed through First-of Class Flight Trials (FOCFT) for every combination of helicopter/ship, to determine Ship Helicopter Operating Limits (SHOL) [2], which detail the safe environmental conditions for launch and recovery operations. FOCFTs are performed at sea and are inevitably very expensive, which can typically take weeks to construct a SHOL envelope and very often the required wind and sea conditions may not be available, resulting in the development of a conservative SHOL [3]. Therefore, Modelling and Simulation (M&S) of the HSDI environment is being developed to examine these risks, making SHOL testing safer, quicker and cost-effective and aims to inform the key test points of high uncertainty to test at sea [4-6]. The reliability of this support depends upon the identification of the fidelity requirements of the M&S elements (Fig. 1), such as the motion and visual cueing, the flight dynamics model and the integration of unsteady airflow to represent the ship's airwake [5]. Attempts have been made to assess the fidelity of the rotorcraft simulators (JSHIP [5]), however, a standardized guideline to quantify the overall simulation fidelity is a challenge which is yet to be fully addressed [7].

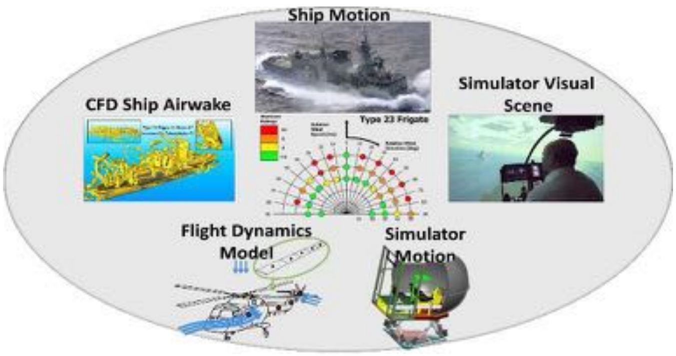

Figure 1: HSDI Modelling and Simulation Elements

Among the core elements of HSDI M&S, vestibular motion cueing is the focus of the research presented here. This has remained an important topic of concern due to a gap in existing knowledge regarding simulator motion fidelity requirements specifically for HSDI operations. Existing literature on motion cueing is primarily focused upon single/multi-axis (not full-axis) based motion assessment and optimisation potentially using frequency domain techniques, pilot subjective opinions or genetic algorithms (GA) [8, 9], which is typically undertaken in the absence of factors such as an unsteady airwake and landing spot movement, which are significant fidelity elements in the HSDI environment. An objective motion fidelity assessment technique OMCT ICAO-9625 is also available to assess the simulator motion fidelity in absence of the pilot and real-world tasks [10]. However, in HSDI operations, unsteady aerodynamic forces act upon the helicopter due to the airwake produced by the wind over the ship. The inclusion of such effects has not been fully examined in the literature. Therefore, further research was required to assess the motion fidelity characteristics and fidelity requirements of simulator motion drive laws for HSDI applications.

Motion cues in a flight simulator are perceived from visual information projected onto the human eye (i.e. visual motion cues also known as vection) and from the simulator's motion platform movement detected by the vestibular system in the human ear and proprioceptive/kinaesthetic cueing [11]. Poor synchronisation of the stimulation and response of optical flow and inertial motion can result in inaccurate vestibular or visual motion cues, leading to vague overall self-motion perception and compromised subjective ratings from the pilots during piloted flight trials [12]. To objectively assess and optimise the vestibular motion cues and determine high fidelity motion cueing for HSDI operations, an offline motion fidelity optimisation technique known as Vestibular Motion Perception Error (VMPE) is proposed in this research (Fig. 2), based on motion perception error minimization strategy. VMPE uses vestibular motion perception models to quantify the difference, or "error", between the vestibular motion perceived by the pilot in the simulator and in the simulated aircraft; this error is minimised for the purpose of motion cueing optimisation.

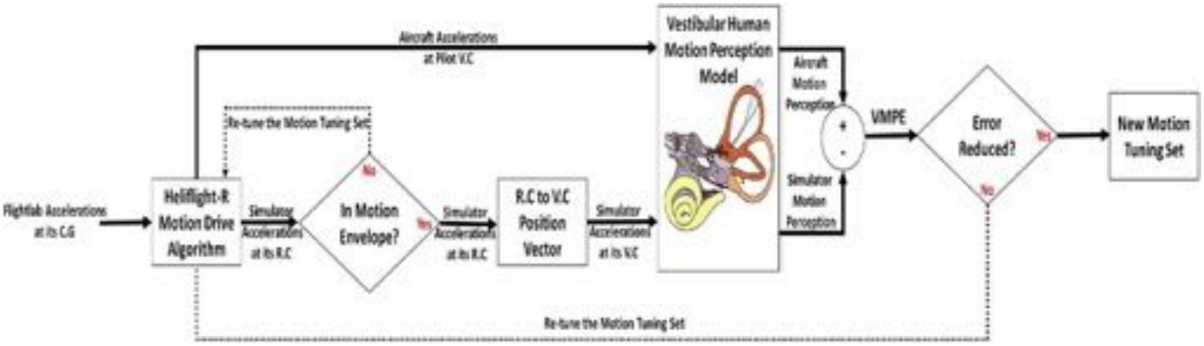

Figure 2: Vestibular Motion Perception Error (VMPE) Technique Architecture

The motion demands of the flight simulator are produced by a motion drive algorithm also known as washout algorithm, as detailed by Reid and Nahon [13]. A generic simulator motion drive algorithm consists of high-pass and low-pass washout filters which attenuate the simulated aircraft accelerations and produce simulator motion demands. The quantity and the quality of the attenuation depend upon the tuning of the filter coefficients: gains, k, and washout frequencies, ω_n, which alter the motion base's response. The collection of these coefficients in all six axes forms a motion tuning set. The proposed VMPE model is incorporated within a Simulink-based motion drive algorithm, Fig. 2. The combined system undergoes a five-step process, which begins with capturing the helicopter accelerations obtained from the FLIGHTLAB model and calculates the simulator motion demands at its rotational centre (RC). The simulator and helicopter accelerations are then transformed to the pilot's vestibular centre (VC) using the position vector. The VC helicopter and simulator accelerations are utilised to estimate the perceived motion by the pilot's vestibular system in helicopter and simulator, using vestibular system transfer functions (acquired from [14]), which are then compared against each other to calculate the VMPE (RMS error) between them. The primary fidelity objective of the simulator is to provide initial accelerations to the pilot which are representative of the real helicopter. Therefore, the VMPE between the two is minimised by tuning the filter coefficients, constraining the simulator excursion in its motion envelope (i.e. 0.6m stroke). The technique has been utilised to optimise the motion cueing in the University of Liverpool's Heliflight-R simulator [7] for an SH60 FLIGHTLAB model landing on the Queen Elizabeth Class aircraft carrier (QEC) at three different airwake conditions (25, 35 and 45kts headwind 'H00'). A subsequent pilot simulated flight trial was conducted to assess the motion perceptions and validate the predictions.

The technique was applied in three phases: Pre-validation, Pre-trial optimisation and Simulated flight trial.

- Pre-validation phase consisted of calculating VMPEs for six motion tuning sets obtained from a surrogate land-based maritime task, Superslide [15] Fig. 3, motion trial conducted in UoL's simulator [8]; which provided multi-axis cueing demands. The VMPEs were compared against the subjective motion fidelity ratings (OMFR) obtained from Jones motion experiment [8], to assess the viability of VMPE technique for future offline pre-trial motion assessment and optimisation, see Fig. 4. The process was repeated for ADS-33E-PRF Pirouette and Lateral Reposition tasks [16]. A similar level of correlation between VMPE estimations and OMFR ratings was obtained in these two cases as well.

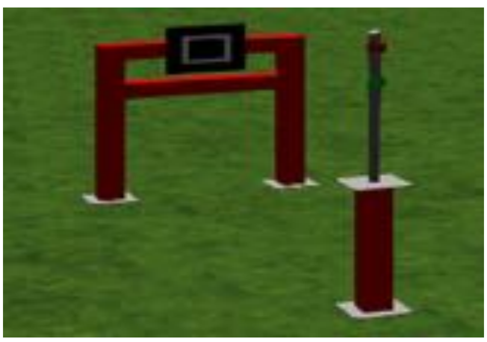

Figure 3: Superslide Course in Heliflight-R Simulator

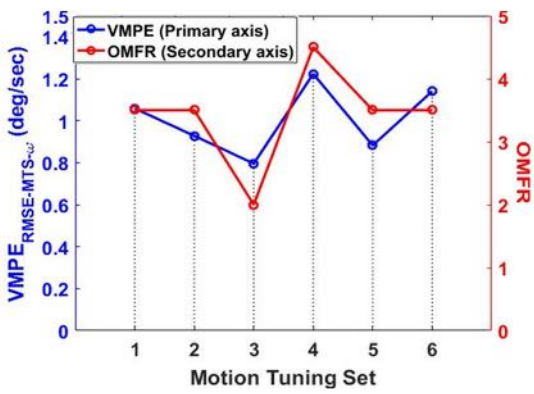

Figure 4: VMPE and OMFR Comparison (Superslide)

- In the optimisation phase, four new motion tuning sets (Benign, Intermediate, Responsive and Optimised) were derived offline for the QEC deck landing task (Fig. 5) at three different wind conditions using the VMPE technique. The helicopter accelerations needed for the optimisation were obtained from a previous non-motion dedicated QEC deck landing flight trial [17]. RMSs of perception errors were calculated individually for each axis, normalised and averaged to determine the VMPE for a motion tuning set. The 'Benign' motion tuning set was predicted to provide the worst motion cueing and 'Optimised' as the best, based on mean motion perception error (black dotted line) minimised from 9.3% to 6.1%, see Fig. 6.

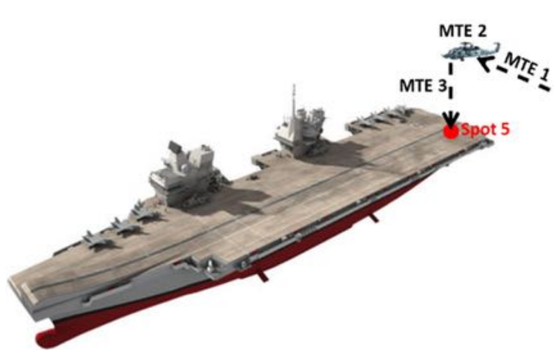

Figure 5: QEC Deck Landing Task to Spot 5

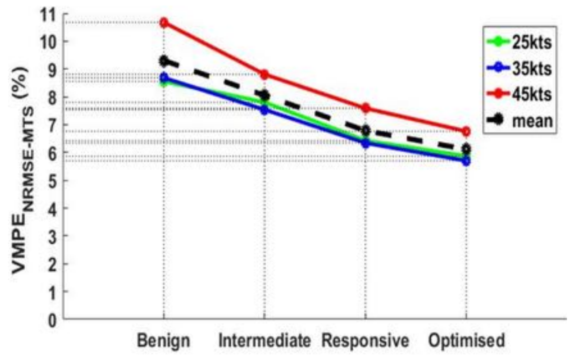

Figure 6: VMPE Results for the QEC Landing Task

- A piloted flight trial was conducted by an experienced former Royal Navy pilot in the HELIFLIGHT-R consisting of twelve QEC deck landings at three Wind over the Deck (WOD) conditions and four new motion tuning sets, obtained within the VMPE optimisation phase. Figure 7 shows the flights trial subjective HMFR results for the twelve cases tested. The coloured region specifies the decision tree regions (High, Medium and Low fidelity) from the HMFR scale proposed by Hodge et al. [9]. An overall agreement was obtained between offline motion optimisation predictions and online simulator flight trial results. The 'Benign' motion set was subjectively rated worst and 'Optimised' as best by the pilot, as predicted during the offline optimisation using VMPE technique (Fig. 6).

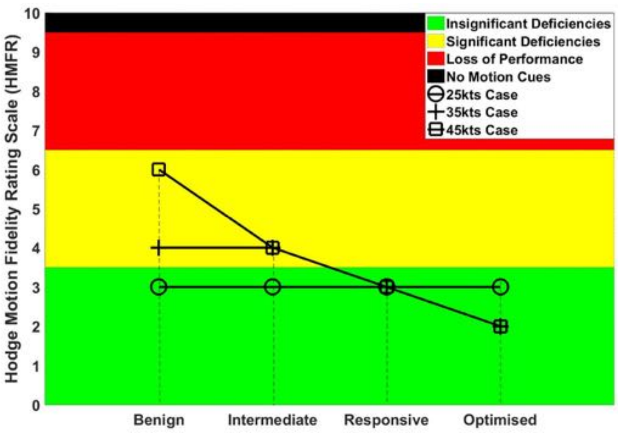

Figure 7: Flight Trial Experiment Subjective Results

Table 1 illustrates the descriptions of a subjective motion fidelity rating scale (HMFR), that has been used to rate the motion cueing by the pilot in the flight trial.

Table 1: Hodge Motion Fidelity Ratings (HMFR) Scale Descriptions [9]

Hodge Motion Fidelity Ratings (HMFR) Scale Descriptions		
HMFR	**Description**	**Decision**
2	Extremely Close to reality, negligible deficiencies	Close to real flight
3	Similar to reality, insignificant deficiencies.	
4	Enhances task performance, slight deficiencies	Not close to real flight
6	Other cues more dominant, annoying deficiencies.	

Figure 8 shows the aircraft trajectories for the two extreme cases, 45kts ‘Benign’ MTS rated HMFR=6 and 45kts ‘Optimised’ MTS rated HMFR=2. An expanded view of the trajectories of the hover MTE is presented in the boxes. It can be seen that the spatial deviation from the hover station-keeping point in the 45kts ‘Benign’ MTS case (blue line) is larger than the 45kts ‘Optimised’ MTS case (red line). This deviation in the ‘Benign’ case is possibly a result of the degraded motion cues which have led to the loss of task performance where the pilot has commented “Poor activity on the controls” and “Poor motion cueing in hover”. Whereas in the ‘Optimised’ case more representative motion cues were provided resulting in better task performance where the pilot has commented “Relatively accurate controls with small inputs”.

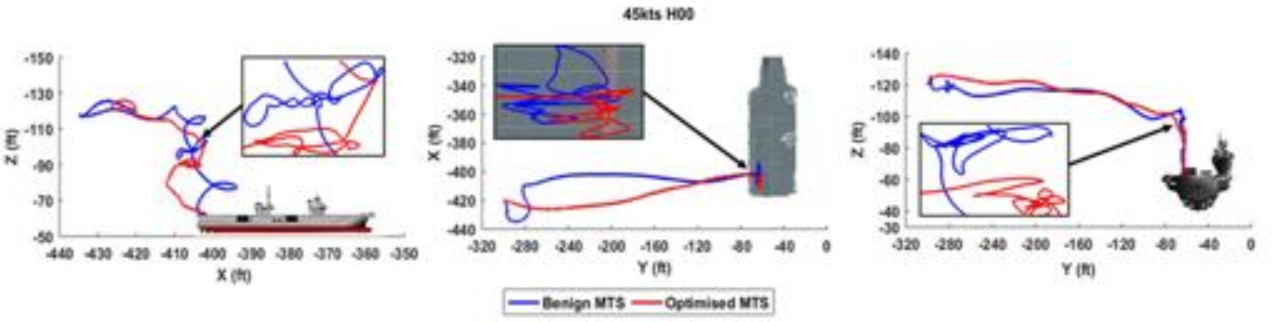

Figure 8: Flight Trial QEC Deck Landing Trajectory

From this motion fidelity study, it was found that the “high-fidelity” vestibular motion cueing becomes more desirable at higher airwake wind conditions than at lower winds, due to higher perturbations in the airflow over and around the ship deck and the subsequent disturbance of the helicopter which the pilot needs to compensate for. The pilot HMFR ratings at 25kts WOD condition remained the same (i.e. HMFR 3-3-3-3) when flying the simulator with any of the four motion tuning sets. However, when the WOD airwake condition was increased to 35kts and 45kts, the motion cueing for the pilot flying the simulator with ‘Benign’ motion set degrades (i.e. HMFR 4-6), while it gets more representative (better) with ‘Optimised’ motion set (i.e. HMFR 2-2).

The results indicated that motion cueing influenced the task performance and the control activity of the pilot. The representative and synchronised vestibular motion cues helped the pilot to perform the task satisfactorily due to the smallest mismatch between vestibular and visual motion cues hence a better overall self-motion perception.

References

[1] Lumsden, B. and Padfield, G. D. “Challenges at the Helicopter-Ship Dynamic Interface,” 24th European Rotorcraft Forum Proceedings, Marseilles, France, September 15-17, 1998.

[2] Fang, R., Krijns, H. W. and Finch, R. S. “Dutch/British Clearance Process,” RTO AGARDograph 300: Helicopter/Ship Qualification Testing, Vol. 22, Flight Test Techniques Series, NATO Research and Technology Organization, 2003.

[3] Forrest, J. S., Owen, I., Padfield, G. D. and Hodge, S. J. “Ship-Helicopter Operating Limits Prediction Using Piloted Flight Simulation and Time-Accurate Airwakes,” Journal of Aircraft, Vol. 49, (4), June. 2012, pp. 1020-1031.

[4] Advani, S. and Wilkinson, C. “Dynamic Interface Modelling and Simulation - A Unique Challenge,” Royal Aeronautical Society Conference on Helicopter Flight Simulation Proceedings, London, November 2001.

[5] Roscoe, M. F. and Wilkinson, C. H. “DIMSS - JSHIP’s M&S Process for Ship helicopter Testing and Training,” AIAA Modeling and Simulation Technologies Conference and Exhibit Proceedings, California, 5-8 August 2002.

[6] Val, J. and Healey, V. “Simulating the Helicopter-Ship Interface as an Alternative to Current Methods of Determining the Safe Operating Envelopes,” NAVAIR: Air Vehicle Division, 1986.

[7] White, M. D., Perfect, P., Padfield, G. D., Gubbels, A. W. and Berryman, A. C. “Acceptance Testing And Commissioning of a Flight Simulator for Rotorcraft Simulation Fidelity Research,” Institution of Mechanical Engineers, Part G: Journal of Aerospace Engineering, Vol. 227, (4), June. 2012, pp. 663–686.

[8] Jones, M. “Application of Motion Tuning Techniques to Rotorcraft Flight Simulation,” RAES Flight Simulation Conference - Striving for Effectiveness in Flight Simulation Proceedings, London, 13-14 June 2017.

[9] Manso, S., White, M. D. and Hodge, S. "An Investigation of Task-Specific Motion Cues for Rotorcraft Simulators," In AIAA Modeling and Simulation Technologies Conference Proceedings, San Diego, California, 2016.

[10] Anon. "Manual of Criteria for the Qualification of Flight Simulation Training Devices," Doc 9625, International Civil Aviation Organization, Third Edition, 2009.

[11] Hosman, R. J. A. W., Cardullo, F. M. and Bos, J. E. "Visual-Vestibular Interaction in Motion Perception," AIAA Modeling and Simulation Technologies Conference Proceedings, Oregon, 08-11 August 2011.

[12] Grundy, J. G., Nazar, S., Omalley, S., Mohrenshildt, M. V. and Shedden, J. M. "The Effectiveness of Simulator Motion in the Transfer of Performance on a Tracking Task is Influenced by Vision and Motion Disturbance Cues," Human Factors, Vol. 58, (4), June 2016, pp. 546–559.

[13] Reid, L., and Nahon, M. "Flight Simulation Motion-Base Drive Algorithm: Part1-Developing and Testing the Equations," UTIAS Report No.296, December 1985.

[14] Nash, C. J., Cole, D. J. and Bigler, R. S. "A Review of Human Sensory Dynamics for Application to Models of Driver Steering," Biol. Cybern, Vol. 110, 2016, pp. 91–116.

[15] Carignan, S., Gubbels, A. and Ellis, K., "Assessment of Handling Qualities for the Shipborne Recovery Task - ADS 33 (Maritime)", 56th American Helicopter Society Annual Forum Proceedings, Virginia Beach, VA, 1-4 May, 2000.

[16] Anon., "Aeronautical Design Standard Performance Specification Handling Qualities Requirements for Military Rotorcraft", ADS-33E-PRF, United States Army Aviation and Missile Command, Redstone Arsenal, AL, 2000.

[17] Kelly, M. F., White, M. D., Owen, I. and Hodge, S. J. "Piloted Flight Simulation for Helicopter Operation to the Queen Elizabeth Class Aircraft Carriers," 43rd European Rotorcraft Forum Proceedings, Milan, Italy, 12-15 September, 2016.

Brown out and White out modeling

Federico Rovere [1], George N. Barakos [2], Rene Steijl [3]
CFD Laboratory School of Engineering, University of Glasgow

Luigi Vigevano [4]
Dipartimento di Scienze e Tecnologie Aerospaziali, Politecnico di Milano

Brownout and whiteout may occur when a rotorcraft is operating in ground proximity. Both the mentioned phenomena are due to the interaction of the rotorcraft wake with the particles of a loose sediment bed. This interaction can eventually cause the uplift of particles (generally sand and dust in the brownout while snow during the whiteout) from the ground and their entrainment into the air flow. When operating in desert areas or in snowy regions, the number of particles entrained can become extremely high creating a cloud around the rotorcraft. The main effects of this cloud of particles moving around the aircraft are on the pilots visual environment and on the rotorcraft structure and equipment. The main objectives of this study is to model these phenomena with CFD, this includes the development of a particle tracking tool in the Lagrangian frame work with one-way coupling assumption and the implementation of the two-phase flow method in the framework of HMB3 CFD solver. Furthermore this project aim to draw concrete conclusions about the importance and role of the parameters affecting brownout through detailed simulations of representative test cases, and based on the obtained results, to calculate the visual impact of brownout and whiteout for a typical operational scenario and assess the impact of brownout and whiteout on the blade and fuselage surfaces.

An important decision when modelling a two phase flow is how to model the dispersed phase, whether sand, snow or water. There are basically two approaches for the numerical simulation of a cloud of particles,and they can be categorised into Lagrangian tracking or Eulerian modelling approaches. In the Lagrangian approach, the particles (or parcels of particles) are tracked through the field and the local cloud properties are defined by their properties as they pass the point in the field. For methods that involves this approach the motion of the particles is tracked solving the Newton's second law. In the case of Eulerian approaches the properties of the particles are assumed to be continuous within the field. Thus, differential conservation equations are written, discredited, and the solution of the resulting set of equations gives the properties of the cloud. A key role in the simulation of brownout is played by the model used to represent the particles uplift. The uplift model used in brownout simulations was first developed Bagnold [1] within the sedimentology community.

One of the main issue trying to model brown out and white out is the simulation of the outflow and the complex flowfield developed around a rotor In Ground Effect (IGE), part of this work is the analysis of the outflow and downflow of a two bladed rotor IGE. Rotors operating in ground effect (IGE) generate complex and unsteady flowfields due to the interaction of the downwash with the ground plane. The result of this interaction is the transition of the rotor induced flow from vertical (downwash) to radial flow (outwash). The test cases simulated were experimentally investigated at the University of Maryland [2]. A detailed analysis of the rotor performances and of the flowfield generated in the experiment will be part of the presentation (Fig 2). Finally, the presentation will include results for the particle tracking, obtained using the Tecplot particle tracking tool (Fig 1) as well as in-house developments.

This project has received funding from the European Union's H2020 research and innovation programme under the Marie Sktodowska-Curie grant agreement No 721920

Bibliography

[1] Bagnold, R., "The physics of blown sand and desert dunes. London: Methuen." 1941.

[2] Lee, T. E., Leishman, J. G., and Ramasamy, M., "Fluid dynamics of interacting blade tip vortices with a ground plane," *Journal of the American Helicopter Society*, Vol. 55, No. 2, 2010, pp. 22005–22005.

[1] PhD Student - federico.rovere@glasgow.ac.uk
[2] Professor - george.barakos@glasgow.ac.uk
[3] Senior Lecturer - rene.steijl@glasgow.ac.uk
[4] Professor - luigi.vigevano@polimi.it

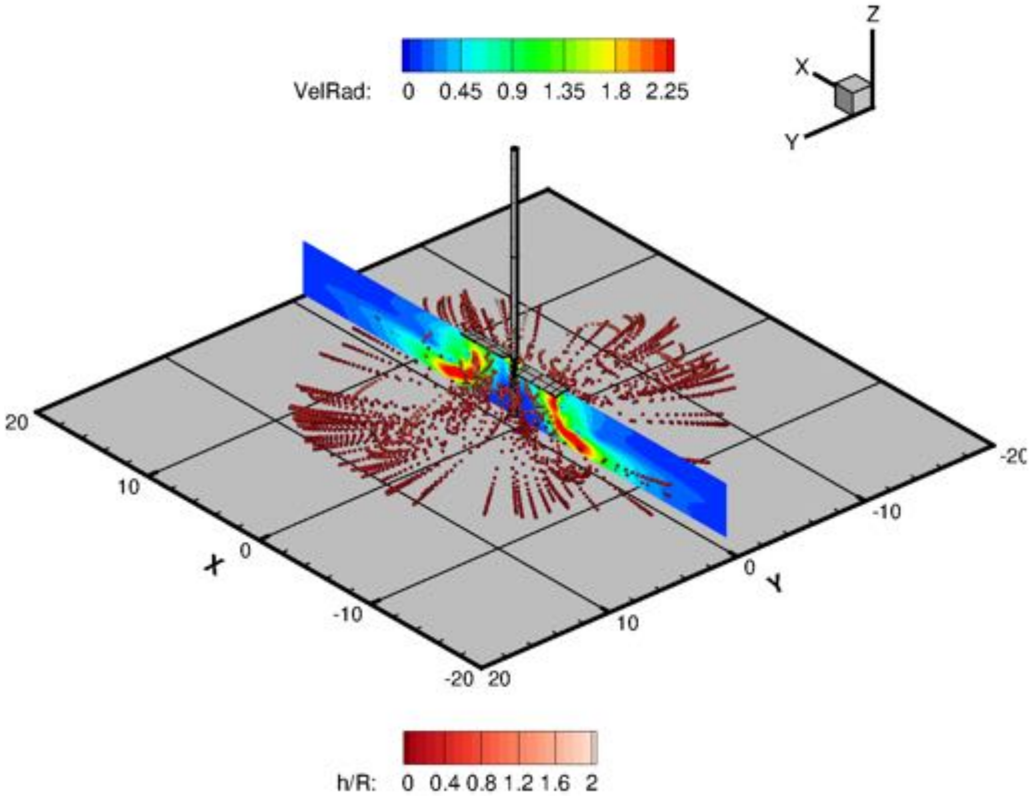

Figure 1: Particle tracking for Lee et al test case [2]. Massless Particles path are calculated over a period of 1.2 seconds, the rotor is operated at $z/R = 1$, $Re_{tip} = 35,000$ and $M_{tip} = 0.08$.

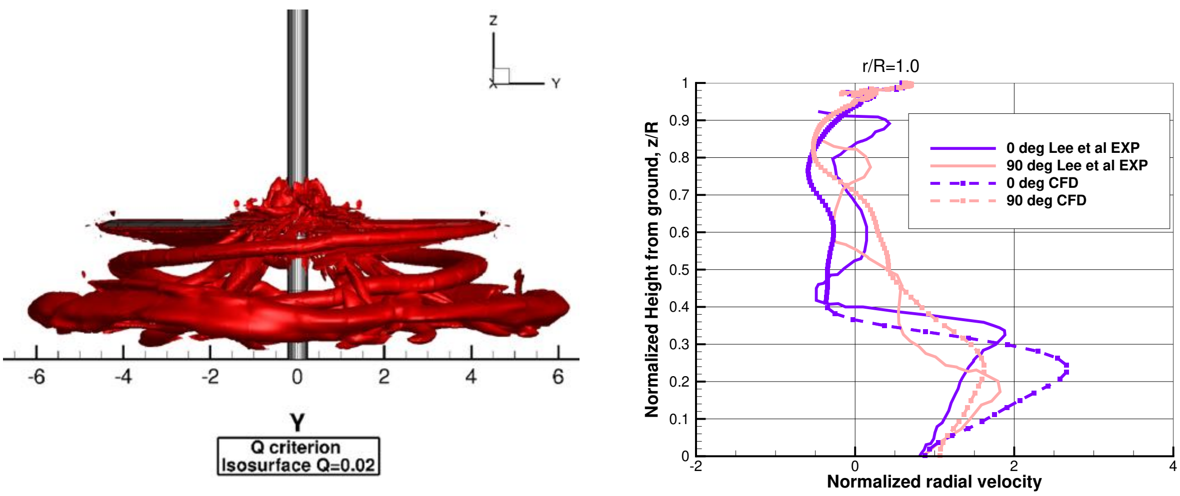

(a) Wake of the rotor (Q criterion)

(b) $r/R = 1$

Figure 2: CFD results for analisys of the outflow for the Lee et al. test Case [2], the rotor is operated at $z/R = 1$, $Re_{tip} = 35,000$ and $M_{tip} = 0.08$.

Aerodynamics of an Open Rotor with a Locked Blade Row

Dale A. Smith*, Antonio Filippone† & George N. Barakos‡

Counter Rotating Open Rotors (CROR) have seen a renewed interest due to their potential to address growing environmental pressures. Due to their high by-pass ratio and without the drag of a duct, the CROR can offer significant fuel savings, and hence, reductions in emissions when compared to modern turbofan engines [1]. Further efficiency gains are achieved by the counter-rotation of the aft rotor, removing residual swirl from the flow. However, with the lack of a duct to limit noise propagation, the noise emission of CROR have so far restricted their application to modern aircraft.

Whilst a number of concepts have been proposed to reduce the interaction noise by modification of the fore rotor wake (e.g. see Refs. [2–7]), it has recently been proposed by the authors to lock a blade row in order to significantly reduce interaction, and hence overall CROR noise. The authors found that locking the aft blade row during take-off, with the fore rotor providing the total required thrust or power, offered significant noise gains over a range of blade count combinations. The locked rotor is then unlocked for normal operation at cruise in order to realise the CROR efficiency gains. The blade row is also locked on approach to reduce noise on arrival.

The authors have been able to demonstrate that noise gains of more than 10 EPNL(dB) can be achieved by locking the aft propeller. The gains were demonstrated using low-order models for both the aerodynamics [8] and acoustics [9, 10]. Whilst these low-order models have been validated for the isolated rotor and the CROR case, the lack of open literature on the case of a locked blade row has limited the ability to verify the results for this case. Therefore, CFD is being used in order to confirm the results that have been obtained. This contribution will present the work carried out by the authors to improve and inform the low-order aerodynamic models for the case of a locked blade row.

In this work, comparisons of the aerodynamics, computed using CFD, of the fully operative CROR and the case with an aft-locked blade row are made, highlighting the reduction in interaction noise mechanisms. The aerodynamics are also compared with the BEMT model in order to highlight areas where improvements in the low-order model are required.

The HMB3 solver [11, 12] has been used to perform CFD computations. The solver has been validated for a wide range of cases, and in particular, propeller flows [13, 14]. It has also been evaluated for the CROR case. Figure 1 compares the flowfield of a 4×4 SR2 [15] CROR computed using the HMB solver and the experimental results of Dunham *et al.* [16]. Note that the CROR was trimmed to match the reported thrust coefficient to within 3.5%. Figure 1 shows that

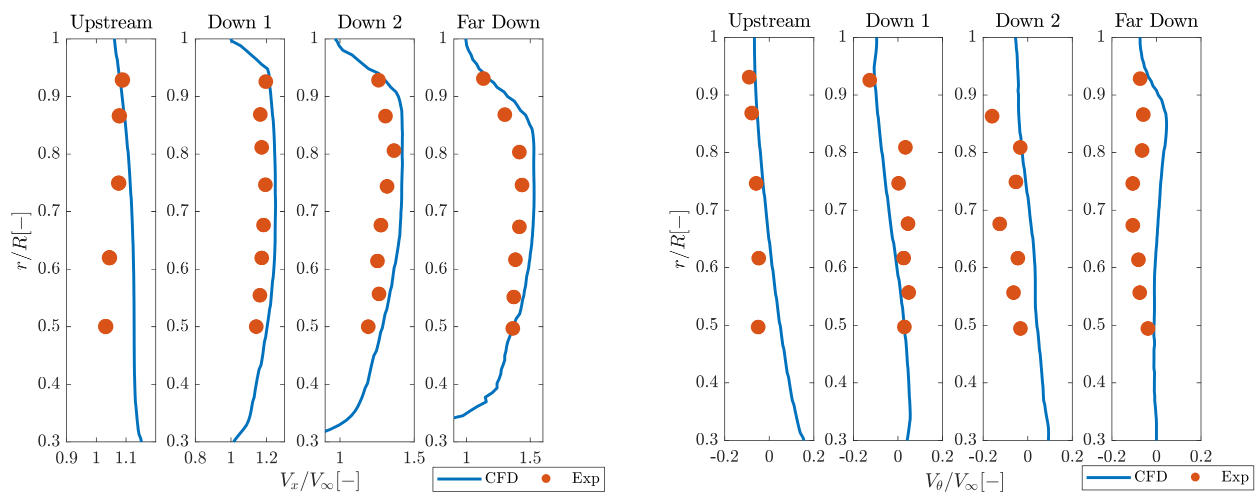

(a) *Normalised axial velocity comparison*   (b) *Normalised radial velocity comparison.*

Fig. 1 CROR CFD Validation

.

HMB has been able to capture the development of the flowfield over the range of axial locations. There is an observed

*PhD Student - dale.smith@manchester.ac.uk - Aviation and the Environment, School of MACE, University of Manchester, UK.
†Reader - a.filippone@manchester.ac.uk - Aviation and the Environment, School of MACE, University of Manchester, UK.
‡Professor - george.barakos@glasgow.ac.uk - CFD Laboratory, School of Engineering, University of Glasgow, UK.

over-prediction in axial velocity. This may be attributed to the increased thrust coefficient the propellers have been trimmed to.

The flow around a 4×4 SR2 [15] CROR has been simulated to investigate the complex aerodynamic flow features of the CROR case. In order to account for the relative motion of each blade, the Chimera overset grid technique [17] has been employed. The blade grid comprised ~ 5 *million* cells. These were then copied to give the full blade count. A background grid, comprising the spinner and far-field was created containing ~ 60 *million* cells. Unsteady Reynolds Averaged Navier-Stokes (URANS) computations are performed, closed by the $k-\omega$ SST model, on both the fully operative case, i.e. $\Omega_1 = \Omega_2$, and the case with aft propeller locked, i.e. $\Omega_2 = 0$. Figure 2 presents axial velocity contours overlaid with iso-surfaces of constant Q-criterion for both cases at an advance ratio of $J = 1.21$.

For the inoperative case, only preliminary results are presented. In previous work, the aft rotor was trimmed to minimise torque, the fore rotor was trimmed to deliver the full torque. In this work, the aft rotor has simply been locked.

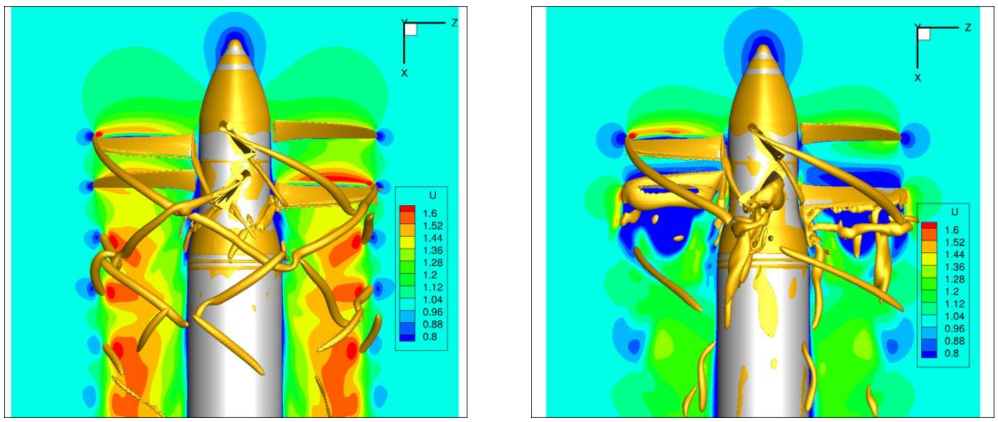

(a) *Operative CROR.*

(b) *CROR with aft-locked row.*

Fig. 2 Slice of axial velocity with iso-surfaces of constant Q-criterion.

As the aft rotor has been locked, it is immediately evident in the reduction in axial momentum in the flow compared to the operative CROR case. This is supported by the reduction in thrust coefficient. For the operative case, $C_T = 0.54$, whilst for the aft-locked case, $C_T = 0.09$. Therefore, it is clear that the aft rotor is creating significant additional drag in this configuration, highlighting the importance of trimming the locked blade row.

Figure 2 also demonstrates some of the interaction mechanisms between blade rows. For example, for the operative case, the tip vortices (shown by the iso-surfaces), merge and separate and continue to do so downstream. For the inoperative case, the fore tip vortex impinges on the aft rotor, with the aft rotor locked, the tip vortex remains almost in the axial direction. Hence, for the operative case, there will more tip vortex interaction than the locked case. For the operative case, interactions occur 8 times per revolution, whilst for the aft-locked case, they occur only 4 times per revolution.

A low-order model has been developed and validated [8] to compute the aerodynamics of CROR. However, with little or no published data for the case of a locked blade row, CFD computations are to be used to inform and improve these existing models. Figure 3 presents the axial and tangential velocity profiles and a number of locations for both CFD and BEMT computations. Figure 3 shows that the BEMT model has predicted a significant negative axial velocity produced by the locked blade row. This results in a disagreement between CFD and BEMT for all axial locations due to the propagation of this component. For the axial velocity components, due to the locked blade row, no induced tangential velocity is predicted by the BEMT model. Therefore, the values reported correspond to the propagation of the induced velocity of the fore rotor. This seems to show some level of agreement with the CFD computations. Therefore, improvements in the prediction in the behaviour of the aft row will result in overall improvements in the BEMT prediction.

This work has presented some preliminary results of the aerodynamics of a CROR with an aft-locked blade row. To proceed, the case of the aft-locked row will be computed where the fore blades are trimmed to deliver the total required thrust, and the aft blades trimmed to minimise torque. Greater insight into the noise generating mechanisms can then be gained and can support the noise reductions previously obtained by the authors. These CFD computations can then to be used to improve the BEMT model. Velocity profiles, like those shown, will be extracted and used to develop more suitable interference coefficients. The behaviour of the aft-locked row, and hence full CROR can then be more accurately captured by the low-order model.

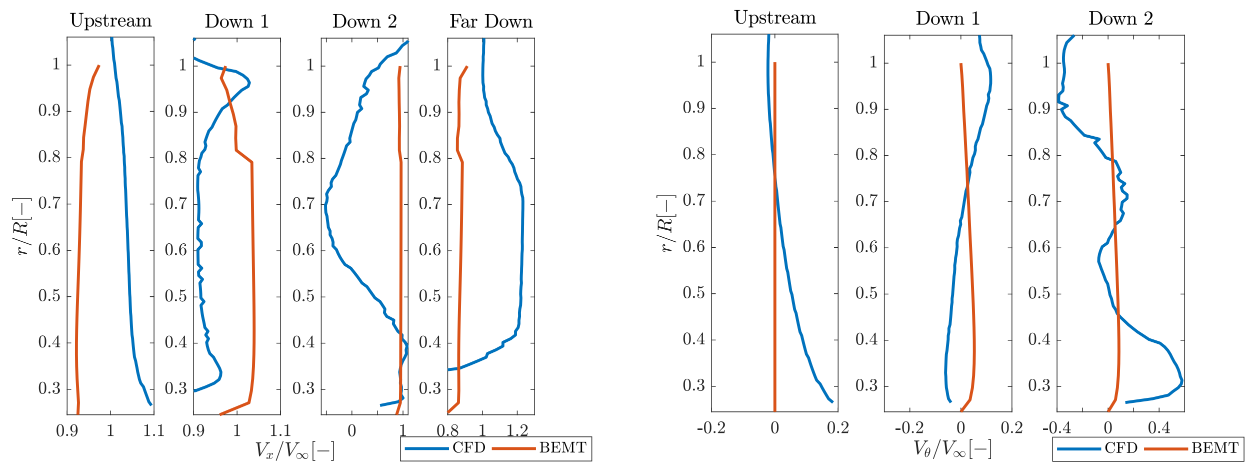

(a) *Normalised Axial velocity.* (b) *Normalised Tangential velocity.*

Fig. 3 Comparison of CFD and BEMT for locked-aft CROR.

Acknowledgements

This research is supported by Mr Mike Newton. The authors would like to extend their gratitude to him for the sponsorship of the work.

References

[1] Zante, D. E. V., "Progress in Open Rotor Research: A U.S. Perspective," *ASME Turbo Expo 2015*, Montréal, Canada, 2015, pp. 1–14. doi:10.1115/GT2015-42203.

[2] Peters, A., and Spakovszky, Z. S., "Rotor Interaction Noise in Counter-Rotating Propfan Propulsion Systems," *Journal of Turbomachinery*, Vol. 134, No. 1, 2010, pp. 2821–2834. doi:10.1115/GT2010-22554, URL `http://proceedings.asmedigitalcollection.asme.org/proceeding.aspx?articleid=1610274`.

[3] Weckmüller, C., and Guérin, S., "On the influence of trailing-edge serrations on open-rotor tonal noise," *18th AIAA/CEAS Aeroacoustics Conference*, 2012.

[4] Zachariadis, A., Hall, C., and Parry, A. B., "Contrarotating Open Rotor Operation for Improved Aerodynamics and Noise at Takeoff," *Journal of Turbomachinery*, Vol. 135, No. 3, 2013, p. 031010. doi:10.1115/1.4006778.

[5] Delattre, G., and Falissard, F., "Influence of Torque Ratio on Counter-Rotating Open-Rotor Interaction Noise," *AIAA Journal*, Vol. 53, No. 9, 2015, pp. 2726–2738. doi:10.2514/1.J053797, URL `http://arc.aiaa.org/doi/10.2514/1.J053797`.

[6] Akkermans, R. A. D., Stuermer, A., and Delfs, J. W., "Active Flow Control for Interaction Noise Reduction of Contra-Rotating Open Rotors," *AIAA Journal*, Vol. 54, No. 4, 2016, pp. 1413–1423. doi:10.2514/1.J053756.

[7] Delattre, G., Falissard, F., Vion, L., and Jacquin, L., "Open rotor interaction noise reduction through front rotor wake modification," *International Journal of Aeroacoustics*, Vol. 15, No. 1-2, 2016, pp. 207–227. doi:10.1177/1475472X16643461, URL `http://journals.sagepub.com/doi/10.1177/1475472X16643461`.

[8] Smith, D. A., Filippone, A., and Bojdo, N., "Low Order Multidisciplinary Optimisation of Counter-Rotating Open Rotors," *European Rotorcraft Forum*, Delft, 2018.

[9] Hanson, D. B., "Noise of Counter-rotation Propellers," *Journal of Aircraft*, Vol. 22, No. 7, 1985, pp. 609–617. doi:10.2514/3.45173.

[10] Parry, A. B., "Theoretical Prediction of Counter-Rotating Propeller Noise," Phd thesis, University of Leeds, 1988.

[11] Barakos, G., Steijl, R., Badcock, K., and Brocklehurst, A., "Development of CFD Capability for Full Helicopter Engineering Analysis," *31st European Rotorcraft Forum*, 2005.

[12] Steijl, R., Barakos, G., and Badcock, K., "A Framework for CFD Analysis of Helicopter Rotors in Hover and Forward Flight." *International Journal for Numerical Methods in Fluids*, Vol. 51, No. 8, 2006, pp. 819–847.

[13] Barakos, G. N., and Johnson, C. S., "Acoustic comparison of propellers," *International Journal of Aeroacoustics*, Vol. 15, No. 6-7, 2016, pp. 575–594. doi:10.1177/1475472X16659214.

[14] Chirico, G., Barakos, G. N., and Bown, N., "Numerical aeroacoustic analysis of propeller designs," *Aeronautical Journal*, Vol. 122, No. 1248, 2018, pp. 283–315. doi:10.1017/aer.2017.123.

[15] Jeracki, R. J., Mikkelson, D. C., and Blaha, B. J., "Wind Tunnel Performance of Four Energy Efficient Propellers Designed for Mach 0.8 Cruise," *NASA TM-79124*, 1979. doi:10.4271/790573.

[16] Dunham, D., Gentry, C. L., and Coe, P. L., "Low-Speed Wind-Tunnel Tests of Single- and Counter-Rotation Propellers," *NASA TM-87656*, 1986.

[17] Jarkowski, M., Woodgate, M. A., Barakos, G. N., and Rokicki, J., "Towards Consistent Overset Mesh Methods for Rotorcraft CFD," *International Journal for Numerical Methods in Fluids*, Vol. 74, 2014, pp. 543–576. doi:10.1002/fld.3861.

SABRE: Shape Adaptive Blades for Rotorcraft Efficiency
Program Overview and Progress to Date

Benjamin K. S. Woods

University of Bristol, Department of Aerospace Engineering, Bristol, BS8 1TR, United Kingdom

SABRE is an H2020 research program investigating the use of blade shape adaptation to improve the efficiency of rotorcraft. It brings together a diverse team of experts from six partner institutions from across the EU. This talk will detail the ambitious dual stream, cross-linked research program that underpins the program and present some promising initial results into the ability of shape adaptation, also known as morphing, to reduce helicopter greenhouse gas emissions by 5 to 11%.

The research program contains a technology development stream where six different morphing concepts and a supporting actuation concept are being developed to allow for real time modification of helicopter blade camber, twist, chord, and dynamic properties. In parallel, a significant amount of rotor level analysis work is taking place to consider the achievable emissions reductions these concepts can produce. These two work streams are connected together using a phased program structure which drives the creation of surrogate models of the morphing technologies which are used within the comprehensive rotor analysis to optimise the achievable reductions in CO_2 and NO_x emissions. Achievable reductions in noise emissions are also being considered.

The shape adaptation devices being investigate include two active camber, two active twist, one chord extension and one active tendon concept which modulates the dynamic response of the blade. Schematics of each of these are in Figure 1.

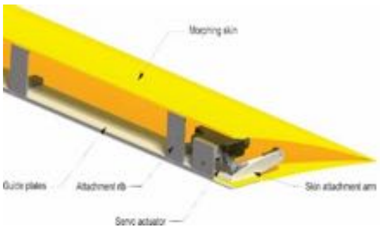

TU Delft – TRIC camber

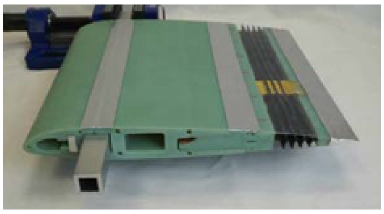

UoB – FishBAC camber

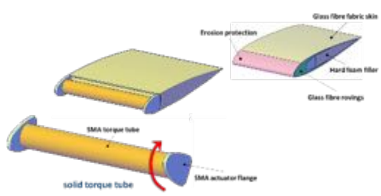

CIRA – SMA twist

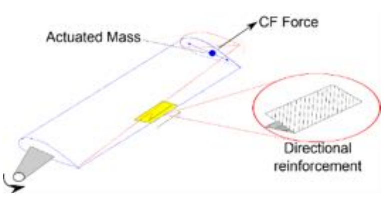

Swansea – inertial twist

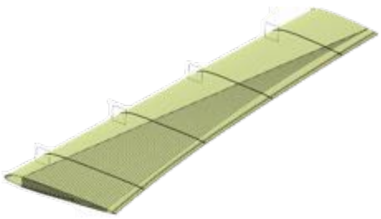

DLR – chord extension

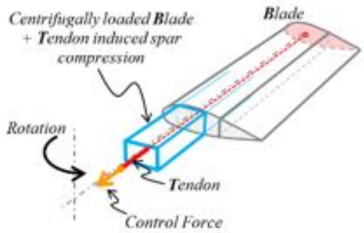

UoB – active tendons

Figure 1. SABRE morphing concepts

Surrogate models of the aerodynamic, mechanical, and inertial behaviour of each of these six concepts have been developed. These models are built around wide-ranging explorations of the concept design space structural and aerodynamic analysis methods which are tailored to each concept and partner, but which must conform to a common interface definition. Specifically: 5 different input variables are required to capture the relevant operating conditions of the morphing devices in hover and forward flight, and 18 different variables capture the resulting performance of the device, including aerodynamic coefficients, stiffness properties in different directions and mass and inertial properties.

Comprehensive rotor analysis has been run for a wide range of morphing rotor conditions. Starting with the properties of the baseline Bo-105 rotor system, the comprehensive analysis includes the physics of the morphing devices by imbedding the surrogate models into the structural, aerodynamic, and inertial property definitions for morphing devices located at different points along the rotor, and operated with different actuation scheduling. Both the DLR developed S4 rotor code and the commercially available CAMRAD II have been used to investigate where each device should be placed on the rotor and how it should be operated to minimise power required and greenhouse gas emissions in both hover (across a range of thrust loadings) and in forward flight (across different advance ratios). Preliminary results have shown the promise of these morphing devices to achieve the stated goals of the program. As seen in Figure 2a, combined chord and camber morphing has shown the ability to reduce hover power requirements by 11%, and in fast forward flight, camber morphing has been shown to provide a 5% reduction in power requirements (Figure 2b).

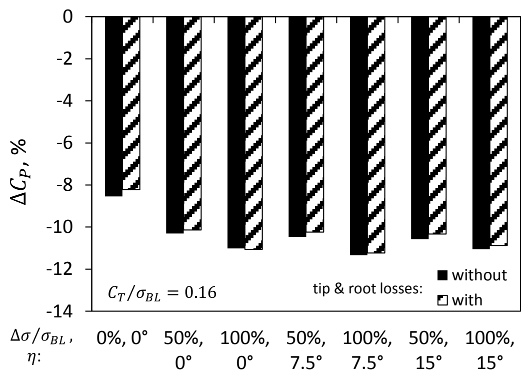

(a)

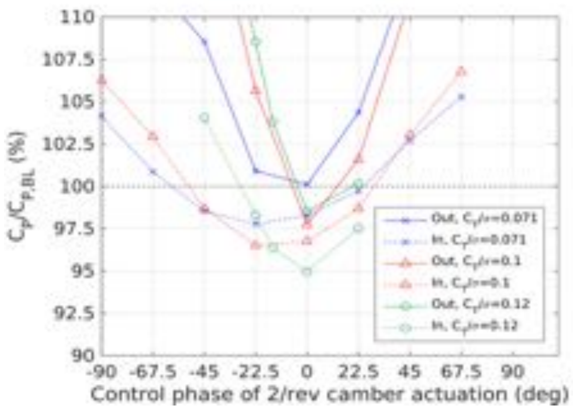

(b)

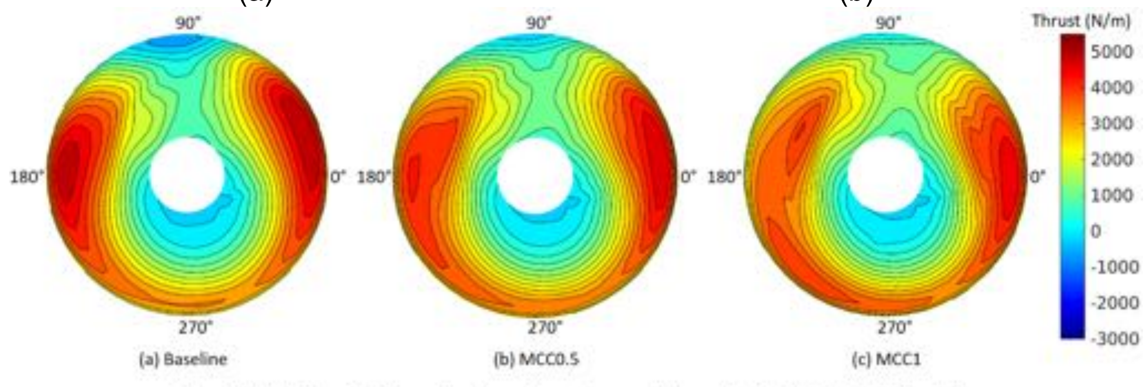

Thrust distribution for 2/rev actuation of camber morphing section 0.5R-0.7R at C_T/σ = 0.1.

(c)

Figure 2: a) Achievable power reductions in hover with chord morphing and camber, b) achievable power reductions with camber morphing in forward flight for different morphing locations and actuator phasing and c) rotor thrust distributions with and without camber morphing, showing more consistent distributions with morphing.

Towards model development for helicopter inceptor dynamics

Mr Edward J.H. Yap, Dr D. Rezgui, Prof. M.H. Lowenberg and Prof. S. Neild

Department of Aerospace Engineering,

University of Bristol, Queens Building, Bristol, BS8 1TR, UK

Dr Khosru Rahman

BAE Systems, Rochester, Kent, ME1 2XX, UK

Summary

The term inceptor refers to the controls pilots use to orientate and manoeuvre an aircraft. Commonly referred to as 'sticks', an inceptor incorporates a whole class of pilot interface controls ranging from centre sticks, side sticks, cyclics, collectives and throttles. An active inceptor introduces the ability to provide tactile force feedback to the pilot [1] with typical anatomies utilising combinations of electrical-mechanical gimbals, springs, actuators, motors, and displacement and force transducers [2]. These components are all interconnected via a network of mechanical links. Understanding how these individual components behave collectively when under the influence of helicopter vibratory loads is crucial in assessing the dynamic response of the entire inceptor unit and maintaining the performance levels required throughout the inceptor unit's service life. This paper investigates the application of a dynamic modelling approach formulated by Udwadia-Kalaba [3] and its potential to predict the dynamic response of a complex multi-body inceptor system. The Udwadia-Kalaba approach is investigated due to its concise formulation approach, simplicity of application [3] and capability of modelling multibody systems subjected to a broad spectrum of constraints, whether they be nonlinear functions of velocities, explicitly dependent upon time or functionally dependent [4].

Initial investigations have largely centred around a test case model system - the Overcentre Mechanism [5] which may be regarded as a crude simplification of an inceptor anatomy involving linkages connected through joints. Simulations comprising analytical, numerical and multi-body dynamic (MBD) approaches were conducted with results validating the Udwadia-Kalaba modelling approach. Additional validation was performed against a model derived using the Lagrange formulation. However, obtaining equations of motion of constrained systems involving large number of degrees of freedom through the Lagrangian may not be pragmatic due to the need to determine the Lagrange multipliers. The equation of motions formulated by Udwadia-Kalaba do not make use or have need for the Lagrange multipliers, which are often difficult to obtain for systems with large number of degrees of freedom [4].

The results obtained demonstrate the nature and applicability of the Udwadia-Kalaba scheme to dynamically model any generic multi-body system subjected to kinematical constraints. Its use is proposed for the inceptor to assess its dynamic characteristics.

Introduction

Inceptors, commonly referred to as 'sticks', incorporate a whole class of pilot interface controls ranging from centre sticks, side sticks, cyclics, collectives and throttles. Active inceptors include the additional ability to provide tactile force feedback from the aircraft control surfaces to the pilot. Whilst typically reserved for military applications [6], there has been a gradual shift in focus to integrate active inceptors within the civilian aviation sector fuelled by some notable high profile events [7]. However, when dealing with fly-by-wire systems, current research trends on aircraft active inceptors have focused predominantly on fixed wing aircraft and as such there is a relative lack of research and guidance associated with active inceptors for rotorcraft applications [8]. Underlying rotorcraft phenomena such as Rotorcraft Pilot Couplings (RPC) and pilot Biodynamic Feedthrough (BDFT) [9,10] showcase a glimpse of the adverse associations that exist between rotorcraft and their vibrations, which continues to be an active field of research [11].


Figure 1: Examples of aircraft inceptor systems. [12]

Typical active inceptor anatomies comprise electrical-mechanical gimbals that utilise combinations of, linear and torsional springs, servo actuators, motors, spherical bearings, ball bearings and displacement and force transducers [2]. These components are all interconnected through a network of mechanical links. Understanding how these individual components behave collectively when under the influence of helicopter vibratory loads is crucial in assessing the dynamic response of the entire inceptor unit and maintaining the performance levels required throughout its service life. Rotary vibration loads are considered the primary design driver within a helicopter [13] however the effects of these harmonic vibrations are difficult to assess; some inceptor system resonances may well fall within the aircraft's operating frequency range and it is imperative that this is avoided.

In early industrial design stages, the dynamic characteristics and performance of an active inceptor cannot be properly assessed nor predicted as this is typically done at the detailed design stage. At early design stages, the inceptor design is said to be in a continual state of change and thus the use of finite element analysis to assess the dynamic behaviour of the full system might not be conclusive or even appropriate. This limitation can present a challenge if significant issues emerge once the inceptor design is finalised, for example system component resonances occurring at or close to the aircraft's forcing frequencies, which can be caused by rotating components such as the main or the tail rotor as specified by the MIL-STD-810G [13] and illustrated in Figure 2. In addition, further iterations in the design cycle may lead in a shift of inceptor component resonances to now occur near the aforementioned forcing frequencies. However, coupled with the requirement to completely rebuild or update models and the adverse impact on industrial project time scales, there is a general sentiment and reluctance within industry to modify an inceptor design upon its finalisation. The drawbacks of this current approach motivate this project to derive an efficiently configurable mathematical model of a candidate active inceptor.

The objective of deriving such a mathematical model of an active inceptor is to provide a means of predicting inceptor mechanism dynamics in the preliminary design stage. The model should be capable of assessing the dynamic characteristics and performance of design layouts to identify acceptable configurations that comply with specified frequency restrictions prior to the later conception of CAD, FE modelling and experimental units. The model must facilitate the evaluation of the inceptor behaviour in terms of design parameters, thus allowing for sensitivity studies and design improvements to be carried out. Thus the development of a suitable mathematical modelling approach would provide an early low-cost means of pre-empting the occurrence of adverse vibration issues as identified above.

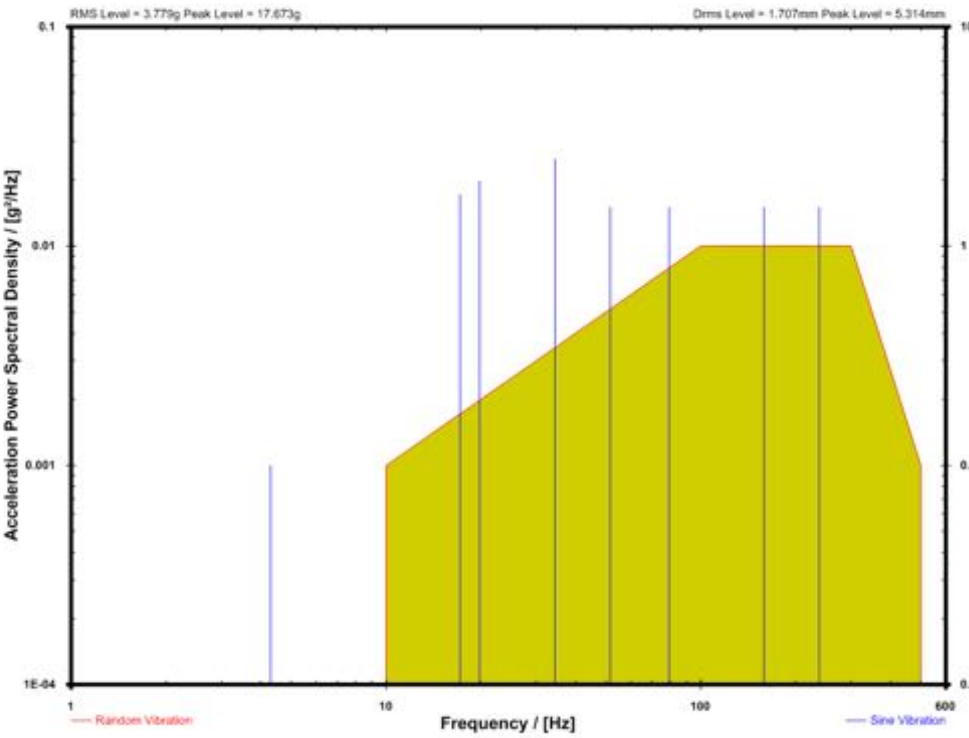

Figure 2: ‘Sine on Random Vibration’ profile for UH-60 Helicopter [13] illustrating a typical vibration profile applied during vibration testing of general components. The main and tail rotor fundamental and blade passing frequencies are superimposed on the low-level wideband random vibration caused by aerodynamic flow.

The Udwadia-Kalaba dynamic formulations

The dynamic equations of motion formulated by Udwadia-Kalaba [3] tackle the issue of multibody mechanical systems subjected to kinematical constraints. The approach reduces such a system to a system of particles and includes the system’s physical geometric constraints as a separate entity. Often referred to as ‘The Fundamental Equation’, the dynamic equation as given by Udwadia-Kalaba [3] is:

$$\ddot{\mathrm{x}}(t) = \mathrm{a} + M^{-\frac{1}{2}}\left(AM^{-\frac{1}{2}}\right)^{+}(\mathrm{b} - A\mathrm{a})$$

$\ddot{\mathbf{x}}$ refers to the true acceleration of the multibody system subjected to geometric constraints. **a** refers to the vector of external accelerations of the multibody system in question purely due to impressed forces acting upon it - often referred to as the accelerations of the ‘unconstrained system’ [3]. $\boldsymbol{M}$ refers to the mass matrix of the considered system. $\boldsymbol{A}$ and $\mathbf{b}$ are matrices obtained from the second-order time differentiation of the system’s constraint equations. $\boldsymbol{A}$ is related to terms associated with state accelerations and $\mathbf{b}$ is associated with state velocities. The combined terms $M^{-\frac{1}{2}}\left(AM^{-\frac{1}{2}}\right)^{+}(\mathrm{b} - A\mathrm{a})$ effectively represent the additional accelerations and subsequent additional force required to ensure the system complies with any kinematical constraint that it is subjected to. This dynamic formulation approach has been investigated by Nielson *et al* [14], Li *et al* [15] and Pennestri *et al* [16] who all found convincing agreement of simulated system dynamic results with reference data.

The Overcentre Mechanism case study

An initial test case model of the Overcentre Mechanism [5] as seen in Figure 3 was considered as an application study of the Udwadia-Kalaba dynamic modelling approach. This model was chosen due to its basic, albeit crude, geometric parallels with that of an inceptor anatomy involving linkages connected through joints. Furthermore, it has been studied previously [5], including its nonlinear characteristics, thus providing a case study for which results could be compared with published data.

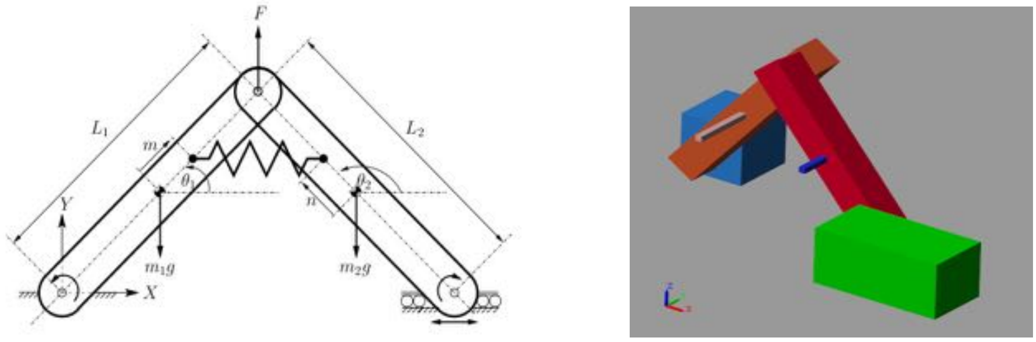

a.) b.)

Figure 3: The Overcentre Mechanism. a) Schematic illustration [5] and b) MBD model representation through MATLAB SimMechanics.

The Overcentre mechanism is two rigid body planar mechanism consisting of six geometric position states (x_1, y_1, θ_1, x_2, y_2, θ_2 where θ_i represents bar rotations and x_i, y_i denotes bar centre of gravity translations as seen in Figure 3). External forcing of varying magnitude was applied and static analysis was conducted using MATLAB formulated from the derivation of the system geometric constraint equations. Results were verified against a second model created within the MATLAB MBD SimMechanics toolkit as presented in Figure 4a.). Effectively validating the system geometric constraint equations used, the dynamic model of the mechanism was formulated within MATLAB based on the Udwadia-Kalaba dynamic approach. The SimMechanics MBD model was used to verify the system dynamic responses formulated from the model based on the Udwadia-Kalaba method.

Results and Discussion

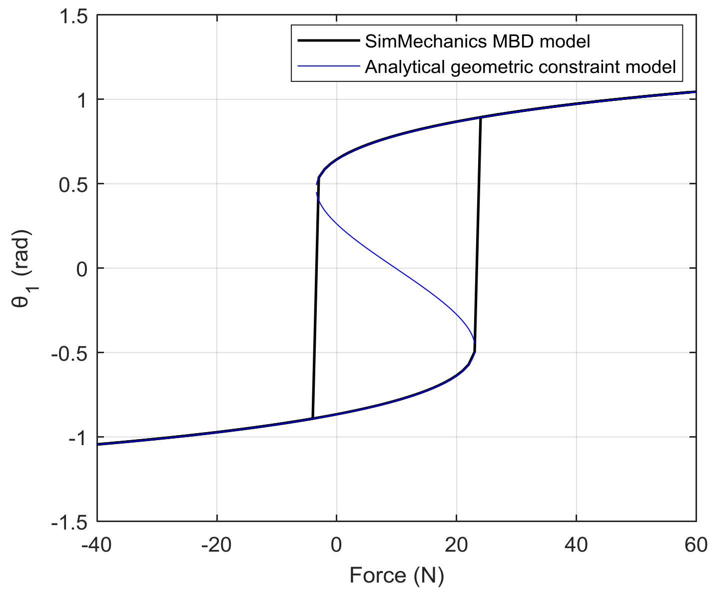

a.)

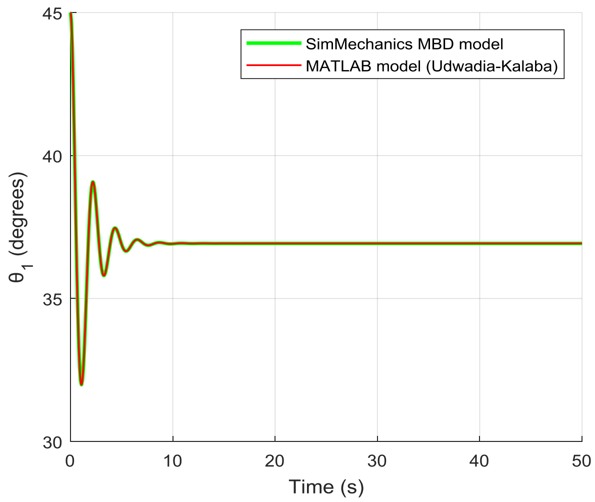

b.)

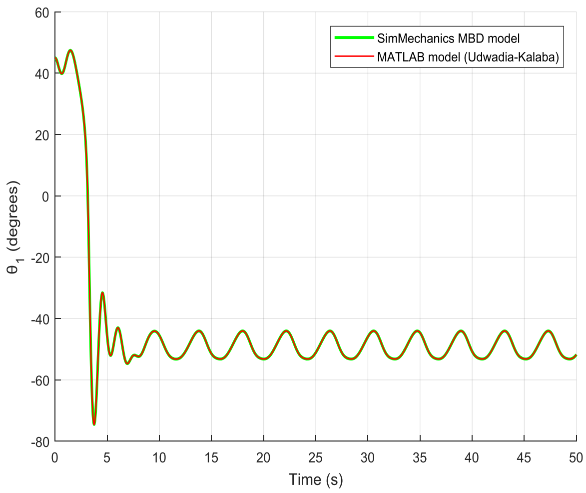

c.)

Figure 4: Overcentre Mechanism responses. a) Static response to a steady force with varying magnitude. b) Free dynamic response of the Overcentre Mechanism (F=0N). c) Dynamic response of the mechanism when subjected to a sinusoidal force (forcing amplitude: 10N, forcing frequency: 1.5 rads^{-1}).

Results from the static analysis of the Overcentre Mechanism in Figure 4a.) show that strong agreement exists between the two modelling approaches. Additionally, it is clear from the results in Figure 4a.) that nonlinearity is present within the system. The appearance of a hysteresis loop is indicative of the system's bi-stability, with the mechanism steady state responses able to switch between the upper and lower branch solutions depending upon whether the applied external force surpasses the respective limit points.

Figures 4b.) and c.) show the dynamic response of the Overcentre Mechanism under free and forced excitation. For the forced excitation case, a sinusoidal force was considered to mimic harmonic vibration loads, as in a helicopter. A forcing amplitude of 10N with forcing frequency of 1.5 rads^{-1} was applied. The strong agreement in Figures 4b.) and c.) between the two modelling approaches verifies the formulations of the dynamic equations used within the Udwadia-Kalaba modelling approach. Comparative studies were also carried out on configurations of the overcentre mechanism that deviated from geometric symmetry. These included combinations of the spring being orientated arbitrarily, differing linkage lengths and arbitrary force application locations along the mechanism. Throughout, strong agreement was observed between the dynamic responses provided from the Udwadia-Kalaba approach and MATLAB MBD toolkit SimMechanics. In agreement with previous studies [14, 15, 16], the results demonstrate the effectiveness and capability of the Udwadia-Kalaba scheme to model any generic multi-body system subjected to kinematical constraints.

Under the project scope, an important objective is to explore the candidate inceptor system's resonant frequency responses. The wider purpose of this is to ensure that the inceptor resonant frequencies do not coincide with the candidate aircraft's forcing frequencies, as illustrated in Figure 2. Drawing parallels with this, a Frequency Response Function (FRF) analysis was conducted on the Overcentre Mechanism case study model to explore the mechanism's theoretical resonant frequency location (1-DoF system), presented in Figure 5.

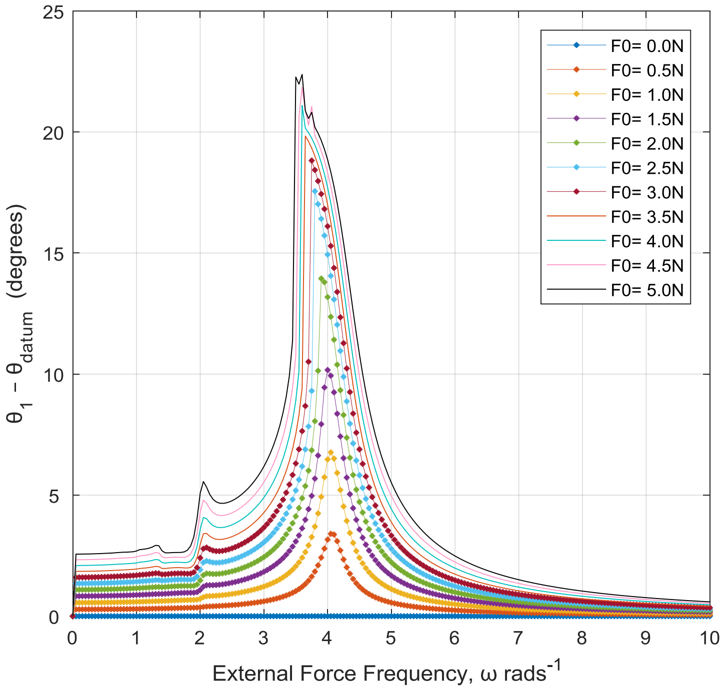

Figure 5: FRF of the Overcentre Mechanism when subjected to a sinusoidal force of increasing forcing amplitudes (F0). Damping coefficient: 1 Nsm^{-1}.

The FRF's in Figure 5 suggest the mechanism's resonant frequency location lies in the region of 4$rads^{-1}$. The findings also demonstrate the capability of the modelling approach to determine the nonlinear nature of the overcentre mechanism in addition to the conclusions derived from the static analysis results in Figure 4a.). In Figure 5, the nonlinear softening effect is observed as system resonant frequency peak locations appear to shift with increasing external forcing amplitudes. Further evidence of nonlinearity is seen with the uneven scaling of system responses with external forcing amplitudes as the height of resonance peaks do not scale in a linear manner.

The candidate inceptor

A physical inceptor unit and its associated data files were provided for this project by BAE Systems. Mathematical modelling of the inceptor's static behaviour was firstly conducted by formulating a MATLAB model based on the system's geometric algebraic constraint equations. Additionally, a SimMechanics MBD model was created. The static analysis concerns itself with investigating the ratio of the inceptor control stick angle with the rotations of the gearbox shaft rotations.

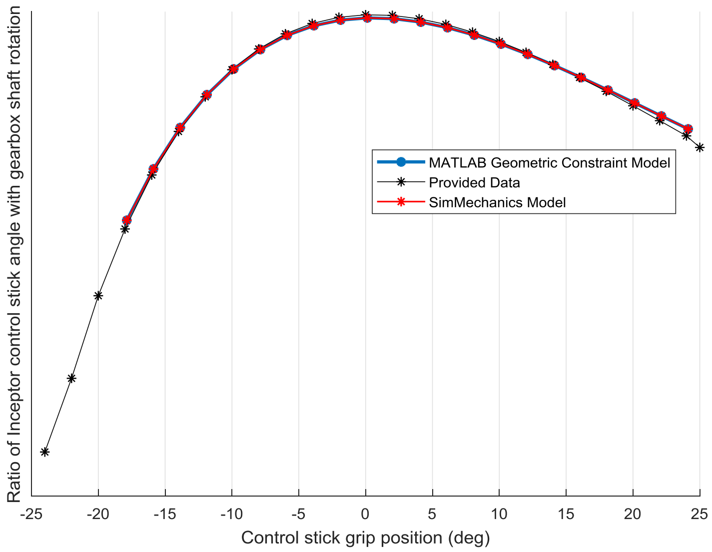

Figure 6: Inceptor static response when stick angle varied. Comparison performed against a geometric algebraic constraint model, an MBD model and data provided by BAE Systems.

As shown in Figure 6, close matching of the MATLAB constraint model and MBD model may be achieved with the provided inceptor data (although exact matching with the latter is challenging due to assumed geometry simplifications and definitions in specific parameter values adopted).

The close nature of inceptor static response behavioural trends observed in Figure 6 between the geometric constraint model with provided data highlights the accurate nature of formulated geometric constraint equations. The fundamental principles governing the Udwadia-Kalaba dynamic modelling approach based on geometric constraint equations may now be transferred and applied to the inceptor to assess its dynamic behaviour.

Conclusions

The ability to assess the dynamic characteristics and performance of an active inceptor is of great importance, and significant advantages accrue if this can be done in its early design stages. Dynamic analysis of the presented case study system, the Overcentre Mechanism, has demonstrated the accuracy and effectiveness of the Udwadia-Kabala dynamic modelling approach for multibody systems subjected to kinematical constraints. Initial static modelling of the sample inceptor system has also produced meaningful results. This approach is now proposed for the dynamic modelling of the inceptor to explore its dynamic characteristics.

Acknowledgment

The research presented in this paper is funded by EPSRC and BAE Systems Plc through an Industrial CASE award (no. 17000065).

References:

[1] Anon. *An Active Role,* BAE Systems, https://www.baesystems.com/en/feature/an-active-role, accessed Feb.,2019.

[2] Anon. *Aerospace Active Inceptor Systems for Aircraft Flight and Engine Controls,* Aerospace Recommended Practice (ARP) 5764, SAE International, 2013.

[3] F.E. Udwadia, R.E. Kalaba, *Analytical Dynamics A New Approach;* Cambridge University Press: Cambridge,1996.

[4] F.E. Udwadia, P. Phohomsiri, *Explicit Poincaré equations of motion for general constrained systems. Part I. Analytical results.* 463**,** Proceedings of the Royal Society A: Mathematical, Physical and Engineering Sciences, 2007.

[5] J. Knowles, *Continuation Analysis of Landing Gear Mechanisms*, PhD thesis, University of Bristol, 2012.

[6] Anon. *Active Inceptor Systems,* BAE Systems Plc. http://www.baesystems-ps.com/pdf/ais_mil_brochure.pdf, accessed Aug.,2018.

[7] Anon. *Air France flight AF 447 Rio de Janeiro-Paris Final Report*, 2012, BEA, https://www.bea.aero/docspa/2009/f-cp090601.en/pdf/f-cp090601.en.pdf.

[8] C.A. Malpica, W. von Grunhagen*, In Flight Evaluation of Active Inceptor Force-Feel Characteristics and Handling Qualities*. Fort Worth, United States. Presented at the American Helicopter Society 68th Annual Forum, May, 2012.

[9] G. Quaranta, P. Masarati, J.Venrooij, *Impact of pilots' biodynamic feedthrough on rotorcraft by robust stability*. Elsevier Science Ltd, Journal of Sound and Vibration 2013;332:4948-4962.

[10] M. D. Pavel, M. Jump, P.Masarati, L. Zaichik, B. Dang-Vu, H.Smaili, G.Quaranta, O. Stroosma, D.Yilmaz, M.Johnes, M.Gennaretti, A.Ionita, *Practises to identify and prevent adverse aircraft-and-rotorcraft-pilot couplings- A ground simulator perspective.* Elsevier Science Ltd, Progress in Aerospace Sciences 2015;77:54-87.

[11] M.D.Pavel, M.Jump, B.D-Vu, P.Masarati, M.Gennaretti, A.Ionita, L.Zaichik, H.Smaili, G.Quaranta, D.Yilmaz, M.Jones, J.Serafini, J.Malecki, *Adverse rotorcraft pilot couplings-Past, present and future challenges.* Elsevier Science Ltd, Progress in Aerospace Sciences 2013;62:1-51

[12] Anon. *Pilot controls- active sticks*, BAESystems, http://www.baesystems-ps.com/pilot-controls.php, accessed Feb.,2019.

[13] Military Standard (MIL STD)- 810G, *Transportation Tailoring Guidance for Vibration Exposure Definition,* Method 514.7, Annex C, 401-403, 2008.

[14] M.C. Nielson, O.A. Eidsvik, M. Blanke, I. Schjolberg, *Validation of Multi-Body Modelling Methodology for Reconfigurable Underwater Robots.* Presented in the OCEANS 2016 MTS/IEEE Monterey conference, IEEE, Sept, 2016.

[15] C. Li, H. Zhao, S. Zhen, H. Sun, K. Shao, *Udwadia-Kalaba theory for the control of bulldozer link lever*. Advances in Mechanical Engineering, 2018.

[16] E. Pennestri, P. P. Valentini, D. de Falco, *An application of the Udwadia-Kalaba dynamic formulation to flexible multibody systems,* Journal of the Franklin Institute, Vol 347, Issue 1, 173-194, 2010.

Helicopter rotor thickness noise control using unsteady force excitation

Yongjie Shi [1]
CFD Laboratory, School of Engineering,
University of Glasgow, G12 8QQ, Scotland, UK

With the wide application of helicopters in military and civilian fields, serious problems concerning noise radiation have been brought to the forefront, emerging as a major factor to be considered in the helicopter design[1]. Among them, the rotor thickness noise which features low frequency, slow attenuation and far-distance propagation, mainly spreads outward along rotor disk plane. It is the major composition of helicopter far-field noise and primary sound detection subject. In past decades, active rotor control has been studied for several years, but most studies were for BVI noise reduction. However, the research on active control for thickness noise reduction is very limited. Gopalan[2] and Sim[3] separately proposed the novel control method for reducing the in-plane noise of the rotor disc in the principle of noise field cancelation and compared the noise reduction effect of single monopole and dipole sources, as well as multiple controllers. Some experimental studies on thickness noise reduction have been carried out as well. Sim[4] conducted an experiment in a wind tunnel test using the Boeing-SMART rotor with active flaps and demonstrated that active flap rotor is possible to reduce in-plane noise. Sargent[5] studied the noise generation mechanism of the tip blowing control and conducted noise tests. In this paper, a noise reduction technique for the rotor thickness noise using a force actuator on blade tip is developed and verified.

As shown in Figure 1, the unsteady aerodynamic force is arranged at the outer portion of the blade to excite a controllable sound wave (anti-noise) opposite to the original noise (thickness noise). The superposition of them could cancel the sound pressure in a certain area, thereby reducing noise. According to the propagation directivity of the force-generated noise, the direction of excitation force should be located in the rotor disk in order to suppress the thickness noise more effectively.

The experiment was carried out in a rotor anechoic chamber in China Helicopter Research and Development Institute. As shown in Figure 2, the anechoic chamber has a spatial size of $30m \times 20m \times 10m$, and the six-sided wall is provided with equipotential metal wedges, the background noise is less than 35dB, and the cut-off frequency is 60Hz. Firstly, we analyses the test result in the condition of first order frequency, 270° initial phase angle and $60 \pm 40V$ voltage (A_f is about 3°). Figure 3(a)- 3(b)gives the contour plot of differential sound pressure level (SPL_on-SPL_off) between baseline and control conditions on the 4m spherical surface of the rotor center. It can be seen that the SPL in the observation area is effectively reduced when the control signal is applied, and the reduction of up to 3dB is achieved in the rotor plane. The time history of sound pressure at 9 microphone is also compared in Figure 4(a)-4(i). When the observations are at the same azimuthal angle (such as P3, P6 and P9 at 180°), the noise reduction in rotor plane is the most obvious (P6), and gradually reduces with the elevation angle increase. The same trend is observed in other azimuths. This is because the anti-noise generated by the trailing edge winglet reaches the largest in the rotor plane. Comparing the observations in the rotor plane (P15, P6, P21), the noise reduction of the observations at 180° is the best, and is less at 150° and 210°.

Then, the effects of the winglet control parameters (frequency, amplitude and phase) on noise reduction are further analyzed in this section. The variation of differential SPL with deflection frequency at P6 microphone is shown in Figure 5(a) , 5(b) and 5(c). The alternating voltage is kept at $60 \pm 40V$. It can be seen that there is an optimal excitation angle at any frequency where the maximum noise reduction can be achieved. When the winglet is excited around this angle, the thickness noise can be effectively reduced, while in other excitation angles, the noise Instead, there will be an increase. The optimal excitation angles correspond to different frequencies. The angle corresponding to the first-order excitation is 300°, and that of the second-order and third-order control are 180° and 90°, respectively.

[1] yongjie.shi@glasgow.ac.uk,shiyongjie@nuaa.edu.cn

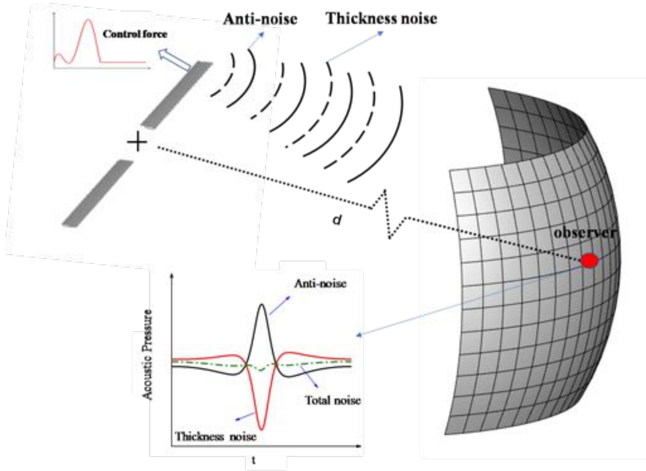

Figure 1: The schematic of noise field cancelation using exciting force

Figure 2: The rotor system and anechoic chamber

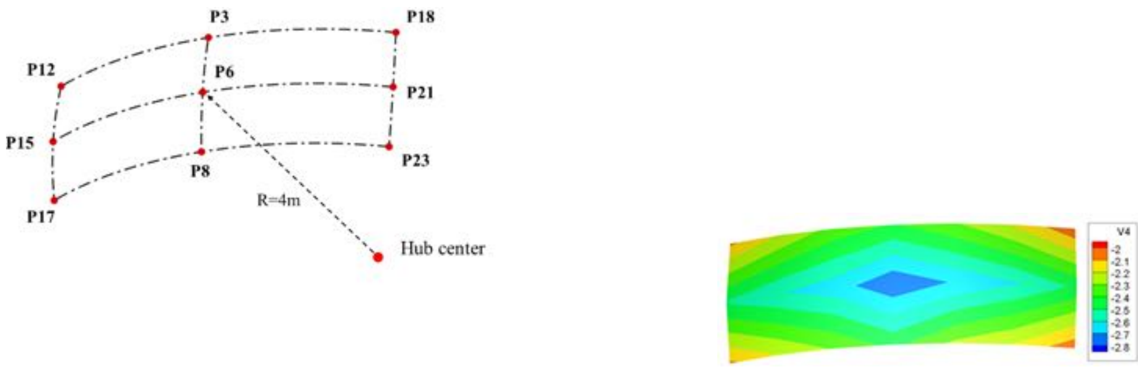

(a) The positions of microphones

(b) contour plot

Figure 3: The contour plot of differential SPL in ftont of rotor

Bibliography

[1] Brentner, K. S. and Farassat, F., "Helicopter noise prediction: the current status and future direction," *Journal of Sound and Vibration*, Vol. 170, No. 1, 1994, pp. 79–96.

[2] Gopalan, G. and Schmitz, F. H., "Low Harmonic Near-In-Plane Far-Field Helicopter Noise Cancellations Using Distributed On-Blade Controls," *AHS Southwest Region Technical Specialists' meeting, Dallas-Fort Worth, TX*, 2008.

[3] Sim, B. W., JanakiRam, R. D., Barbely, N. L., and Solis, E., "Reduced in-plane, low frequency noise of an active flap rotor," Tech. rep., 2009.

[4] Sim, B. W., JanakiRam, R. D., and Lau, B. H., "Reduced In-Plane, Low-Frequency Noise of an Active Flap Rotor," *Journal of the American Helicopter Society*, Vol. 59, No. 2, 2014, pp. 1–17.

[5] Sargent, D. C. and Schmitz, F. H., "Fundamental Experimental Studies Supporting Active-Jet Acoustic Control of In-Plane Rotor Harmonic Noise," *Journal of Aircraft*, Vol. 51, No. 2, 2014, pp. 434–446.

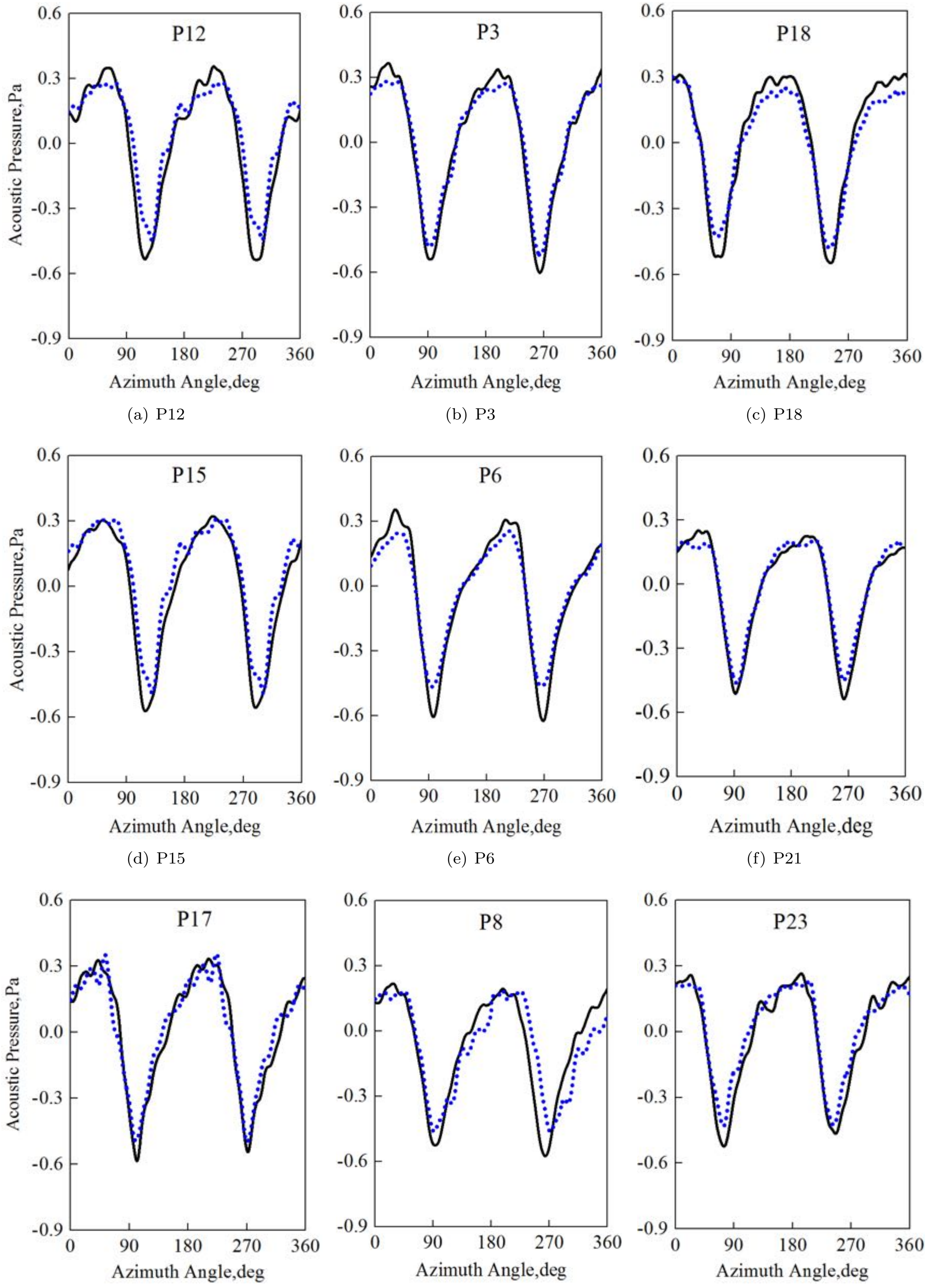

(a) P12 (b) P3 (c) P18

(d) P15 (e) P6 (f) P21

(g) P17 (h) P8 (i) P23

Figure 4: The noise reduction in the condition of n=1Ω,A_f=3°,Ψ=270°

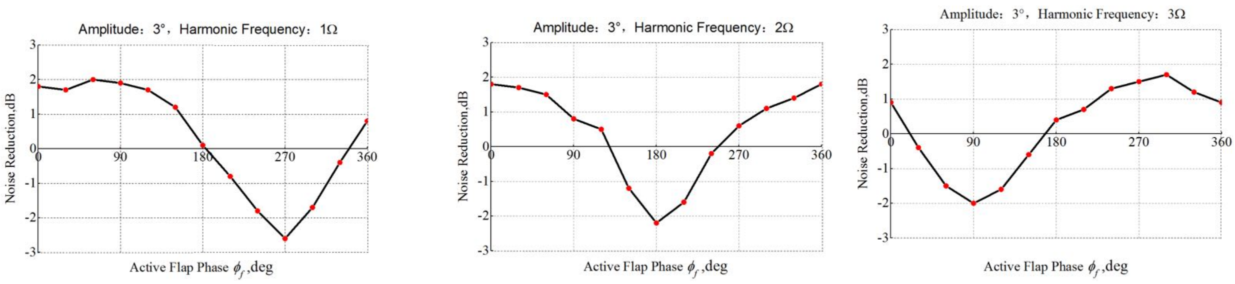

(a) H_f=1 (b) H_f=2 (c) H_f=3

Figure 5: The differential SPL varies at P6 microphone with deflection frequencies

4^{th} Vertical Lift Network Workshop, 8-9^{th} April 2019, Cheshire, United Kingdom

Experimental investigation of a two-bladed propeller at yaw

Angel Zarev	Ross Higgins	Richard Green
University of Glasgow	University of Glasgow	University of Glasgow
PhD student	PhD student	Senior lecturer

1 Abstract

After decades in the shadow of turbofans and turbojets, the focus of a large section of the aeronautical sector is slowly shifting back to propeller based propulsion. One of the aspects of propeller propulsion left largely unexplored is their behaviour when exposed to an incident airflow. There are no recent or accurate studies on the topic and most of the widely used mathematical models still work under the assumption of uniform induced flow distribution across the disc, laid out by de Young [3] 53 years ago, or the 'steady-state' assumption, laid out by Crigler [2] 66 years ago. Studying the inflow of propellers at incidence is an opportunity to provide a solid foundation for validation of numerical methods, while also highlighting any gaps in the studies performed so far.

To this end, an experimental investigation has been performed in the $2.06 \times 2.66\,m$ De Havilland National Wind Tunnel Facility to measure inflow into a two-bladed propeller over a range of five advance ratios and five yaw angles. The measurements were conducted using a three-component Laser Doppler Anemometry (LDA) one chord away from the propeller plane over a coordinate grid of 396 points. The results have been converted into propeller axial, tangential, and radial induction factors and compared against widely used engineering level mathematical models of propellers at incidence [1, 2]. Preliminary investigation of the results demonstrates that the aforementioned methods fail to correctly predict inflow distribution over the propeller plane. This puts in question the ability of said methods to determine forces over the propeller plane itself.

The presentation will encompass the motivation behind the research, experimental methodology, notable data trends of propellers at incidence, comparison between experimental results, mathematical models (including CFD), and future research aims.

2 Experimental results sample

Demonstrated in fig.1 is the propeller induced axial induction factor at 20 ° incidence. Observing this, it can easily be discerned why assuming uniform induced flow across the disk has little physical basis. Furthermore, it can clearly be seen that both the maxima and minima are lagging behind their respective advancing and retreating peak positions, where according to steady-state wake theory as presented by Crigler [2] - they should be situated; with maxima and minima at 180 ° and 0 °, respectively.

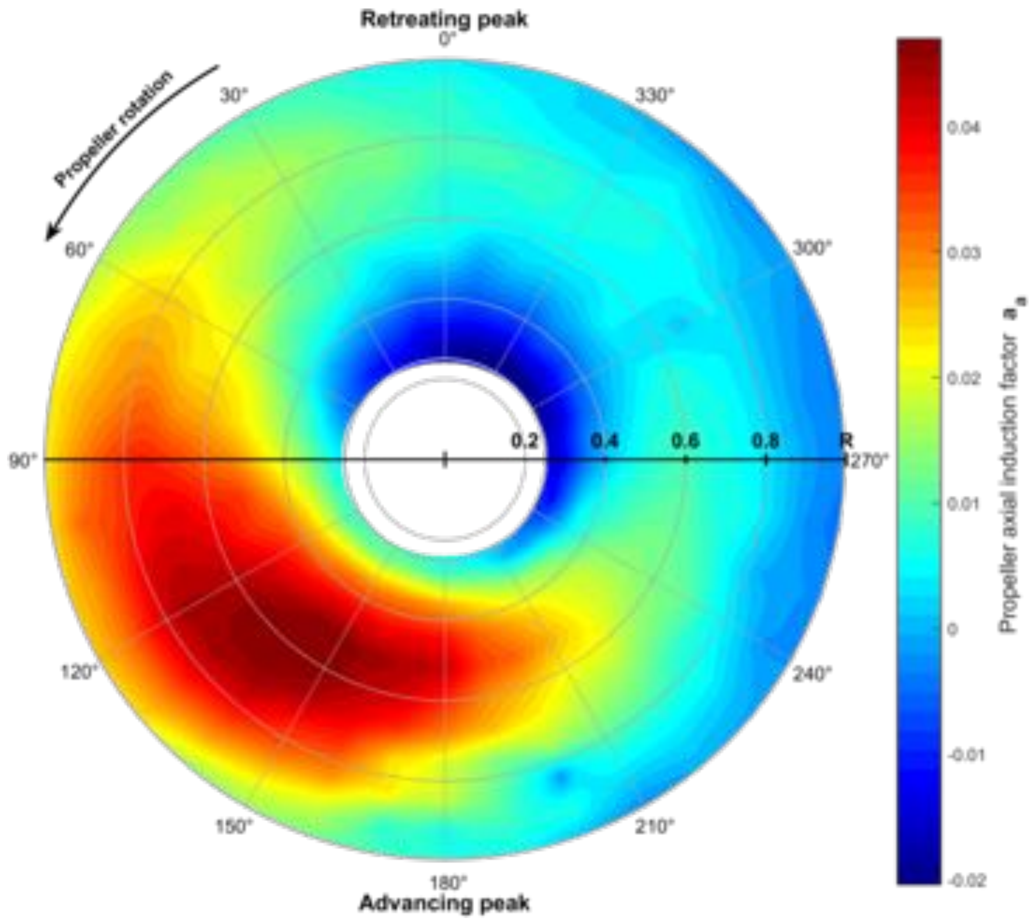

Figure 1: Propeller induced axial induction factor
J = 1.57, $V_\infty = 30\ m/s,\ \theta = 20\ °,\ \beta = 49\ °,\ RPM = 2342$

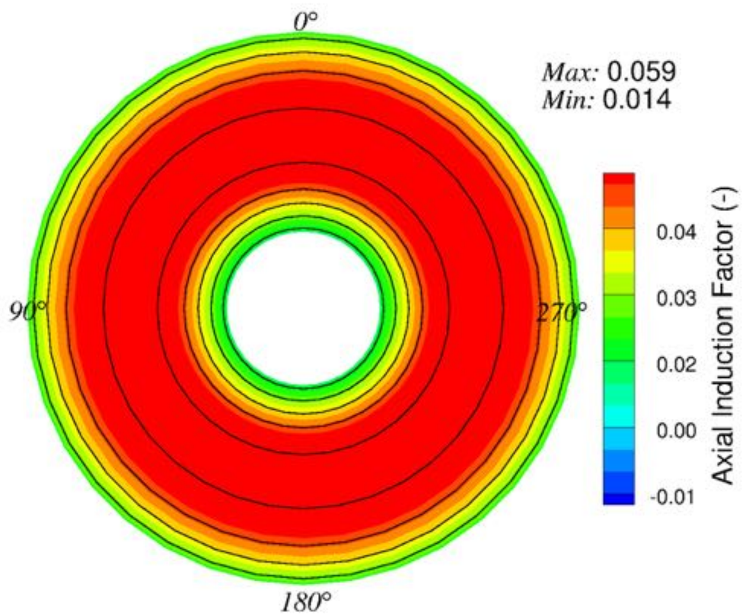

(a) CDF

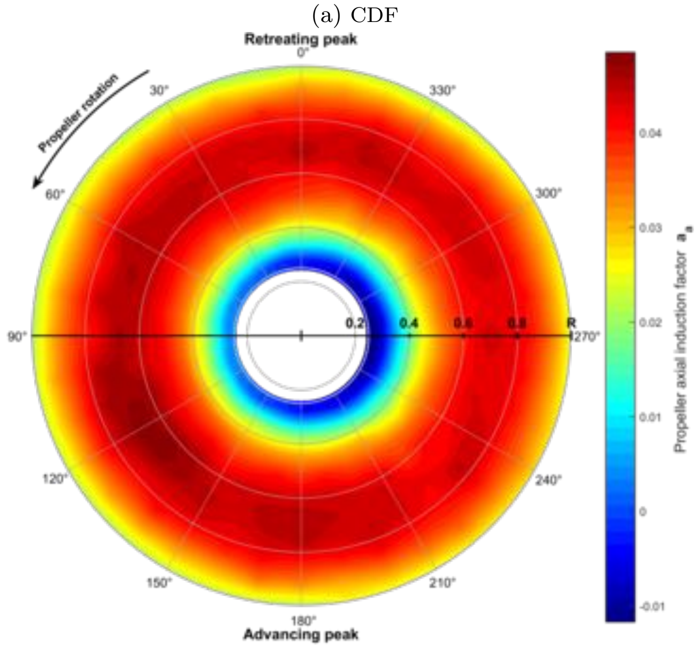

(b) Experimental

Figure 2: Initial CFD results comparison
$J = 0.89,\ V_\infty = 20\ m/s,\ \theta = 0\ °,\ \beta = 28\ °,\ RPM = 2756$

3 Acknowledgements

References

[1] P. D. Chappell. *In-plane forces and moments on installed inclined propellers at low forward speed.* ESDU, 1989.

[2] John L Crigler and Jean Gilman Jr. Calculation of aerodynamic forces on a propeller in pitch or yaw. Technical report, NATIONAL AERONAUTICS AND SPACE ADMINISTRATION WASHINGTON DC, 1952.

[3] John De Young. Propeller at high incidence. *Journal of Aircraft*, 2(3):241–250, 1965.

Towards Optimisation of Compound Rotorcraft

Tao Zhang [1] and George N. Barakos [2]
CFD Laboratory, School of Engineering,
University of Glasgow, G12 8QQ, Scotland, UK

Compound rotorcraft is a generalisation of the term compound helicopters. According to Graham[1], compound is "a rotorcraft which, in flight, and at slow speed derives the substantial proportion of its lift from a rotary wing system but at speed can generate lifting and longitudinal thrust from a suitable combination of rotary wing system, fixed lifting surface(s) and auxiliary propulsor(s)". A rotorcraft of this type possesses, simultaneously, the high-speed performance of a fixed-wing plane and the hover efficiency of a conventional helicopter, and is ideal for use as emergency/medical evacuation or urban taxi. So compound rotorcraft can bridge the gap between traditional helicopters and fixed-wing aircraft, and fill the mission gap between airplanes and conventional low-speed helicopters[2].

However, the fuselage, the main rotor(s), the auxiliary wing/tail, and the ducted or open propeller(s) bring significant aerodynamic interactions, and may lead to severe control/trim difficulties, vibration/stability concerns and etc. While the optimum design of compound rotorcraft needs careful arrangement of each component to have optimal performance under specific constraints. It is expected that the joint use of modern high-fidelity CFD methods and gradient-based adjoint methods represents a powerful approach, through which the complex aerodynamic interactions can be resolved and studied, and the optimised configuration can be decided.

This paper begins with a literature survey into the development of compound rotorcraft and ducted fans. A compound helicopter model is also assembled, consisting of a parameterised Dauphin-like fuselage, ducted fans for auxiliary thrust, and a main rotor. Resolving the rotor and propeller blades involved certainly requires large scale CFD computation. Nevertheless, to study the interactions between rotor wake/fuselage/ducted fan, an unsteady actuator line is proposed. Figures 1(a) and 1(b) show the mesh topology with resolved blades or with unsteady actuator disks, while Figure 2 shows the main rotor wake at low advance ratio. As shown in Figure 2, the method can model the complex rotor wake structure with efficiency. To validate the HMB3 and adjoint methods[3], a ducted fan tested by NASA[4] is used. Since very few data is given[4], comparisons were also made against the method of M. Drela[5][6]. Figures 3(a) and 3(b) show good correlation between the methods for pressure distributions along the center-body and duct. Gradient-based duct shape optimisation for higher thrust is also studied. A detailed analysis of the obtained results for the compound rotorcraft, as well as, for the validation of HMB3 for flows in ducted fans, is presented in the full paper.

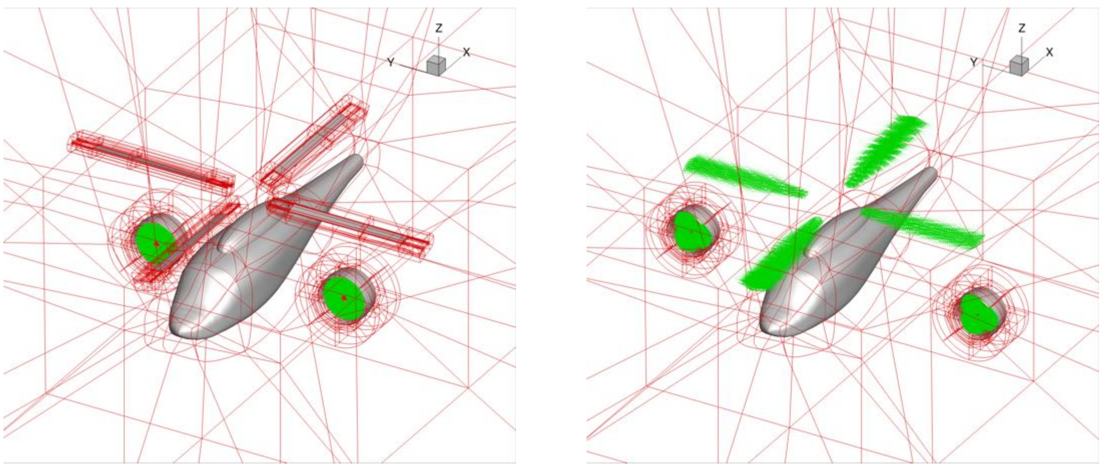

(a) Grid topology with blades

(b) Grid topology with unsteady actuator lines

Figure 1: Multi-block mesh topology

[1] PhD Student - 2354711Z@student.gla.ac.uk
[2] Professor - george.barakos@glasgow.ac.uk - corresponding author

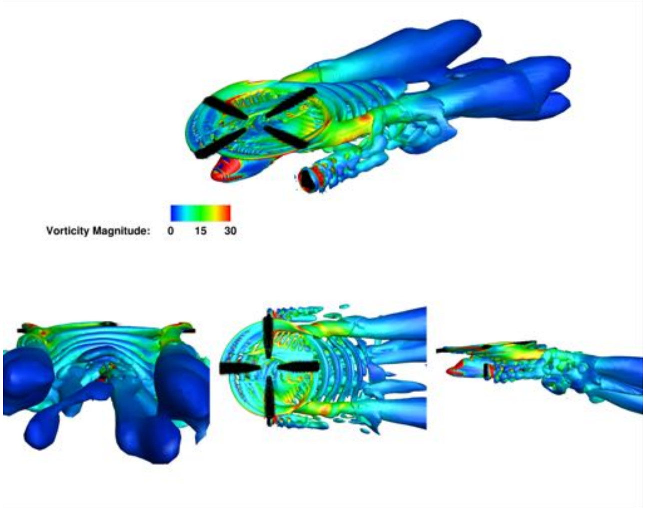

Figure 2: Wake structure obatined from unsteady, non-uniform actuator disks (iso-surface of Q=0.5, colored by vorticity),

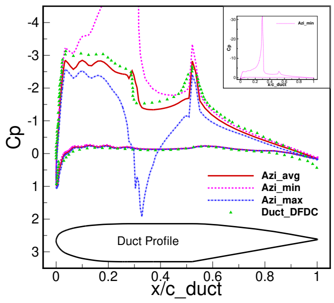

(a) Cp distribution on the duct

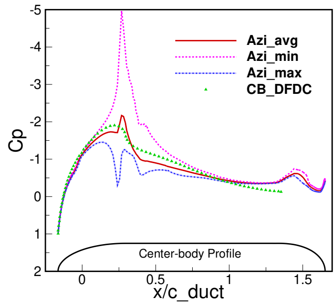

(b) Cp distribution on the center-body

Figure 3: Pressure coefficient distributions along the duct and center-body surface of the NASA configuration[4]. The peak and averaged values predicted by HMB are compared with the method of M. Drela[5][6].

The sponsorship of the University of Glasgow and the China Scholarship Council is gratefully acknowledged.

Bibliography

[1] Graham, J., "Definition of a Rotorcraft," `https://www.aerosociety.com/Assets/Docs/Publications/SpecialistPapers/Definition_of_a_Rotorcraft.pdf`, Februry 2013, Special paper of the Royal Aeronautical Society, available on-line.

[2] Ormiston, R. A., "Revitalising advanced rotorcraft research - and the compound helicopter ," *The Aeronautical Journal*, Vol. 120, 2016, pp. 83 – 129.

[3] Biava, M., Woodgate, M., and Barakos, G. N., "Fully implicit discrete-adjoint methods for rotorcraft applications," *AIAA Journal*, Vol. 54, No. 2, 2015, pp. 735–749.

[4] Grunwald, K. J. and Goodson, K. W., "Aerodynamic Loads on an Isolated Shrouded-propeller Configuration for Angles of Attack from -10 Degrees to 110 Degrees," Tech. rep., National Aeronautics and Space Administration Washington DC, 1962.

[5] Youngren, H., Drela, M., and Sanders, S., "Ducted Fan Design Code," `http://web.mit.edu/drela/Public/web/dfdc/`, December 2005, Ducted Fan Design Code homepage, available on-line.

[6] Drela, M. and Youngre, H., "Axisymmetric Analysis and Design of Ducted Rotors," `http://web.mit.edu/drela/Public/web/dfdc/DFDCtheory12-31.pdf`, December 2005, Ducted Fan Design Code theory, available on-line.